NONOSCILLATORY CENTRAL SCHEMES FOR MULTIDIMENSIONAL HYPERBOLIC CONSERVATION LAWS*

GUANG-SHAN JIANG† AND EITAN TADMOR‡

Abstract. We construct, analyze, and implement a new nonoscillatory high-resolution scheme for two-dimensional hyperbolic conservation laws. The scheme is a predictor-corrector method which consists of two steps: starting with given cell averages, we first predict pointvalues which are based on nonoscillatory piecewise-linear reconstructions from the given cell averages; at the second corrector step, we use *staggered* averaging, together with the predicted midvalues, to realize the evolution of these averages. This results in a second-order, nonoscillatory *central* scheme, a natural extension of the one-dimensional second-order central scheme of Nessyahu and Tadmor [*J. Comput. Phys.*, 87 (1990), pp. 408–448].

As in the one-dimensional case, the main feature of our two-dimensional scheme is *simplicity*. In particular, this central scheme does not require the intricate and time-consuming (approximate) Riemann solvers which are essential for the high-resolution upwind schemes; in fact, even the computation of the exact Jacobians can be avoided. Moreover, the central scheme is "genuinely multidimensional" in the sense that it does not necessitate dimensional splitting.

We prove that the scheme satisfies the *scalar maximum principle*, and in the more general context of systems, our proof indicates that the scheme is *positive* (in the sense of Lax and Liu [*CFD Journal*, 5 (1996), pp. 1–24]). We demonstrate the application of our central scheme to several prototype two-dimensional Euler problems. Our numerical experiments include the resolution of shocks oblique to the computational grid; they show how our central scheme solves with high resolution the intricate wave interactions in the so-called double Mach reflection problem [*J. Comput. Phys.*, 54 (1988), pp. 115–173] *without* following the characteristics; and finally we report on the accurate ray solutions of a weakly hyperbolic system [*J. Comput. Appl. Math.*, 74 (1996), pp. 175–192], rays which otherwise are missed by the dimensional splitting approach. Thus, a considerable amount of simplicity and robustness is gained while achieving stability and high resolution.

Key words. hyperbolic conservation laws, multidimensional systems, central difference schemes, nonoscillatory schemes

AMS subject classifications. Primary 65M10; Secondary 65M05

PII. S106482759631041X

Contents.

1. Introduction. We study the approximation of two-dimensional conservation laws by second-order accurate, nonoscillatory *central* difference schemes. The main feature of our central schemes is *simplicity*: since no (approximate) Riemann solvers and related characteristic decompositions are involved, we derive efficient, genuinely multidimensional schemes, which are independent of dimensional splitting.

The construction of our central scheme in the prototype two-dimensional case is carried out in section 2. It amounts to a simple two-step predictor-corrector method outlined in (2.15)–(2.16) below. In section 3 we carry out the stability analysis which proves that the two-dimensional scheme satisfies the *scalar maximum principle*. In fact, our arguments indicate that in the more general context of multidimensional *systems*, the central scheme satisfies the *positivity condition* of Liu and Lax [LL]. Finally, we implement the proposed central scheme for a variety of prototype two-dimensional problems, whose results are reported in section 4. In particular, we would like to highlight the following.

- *Scalar equations.* The nonoscillatory behavior of the scalar results is found to be in agreement with the maximum principle indicated above.
- *Two-dimensional systems.* Three canonical problems are considered: the rotated Riemann problem, the double Mach reflection problem, and a 2×2 *weakly* hyperbolic system introduced by Engquist and Runborg, which arises in the macroscopic closure of a multiphase geometrical optics expansion [ER]. The numerical results demonstrate the nonoscillatory, high-resolution content of our proposed central schemes. It is in this context of *systems* of conservation laws that the simplicity and flexibility of our central schemes are translated into *efficiency*. Specifically, one can avoid the time-consuming computation of (approximate) Riemann solver(s) and the related characteristic decompositions; in fact, even the (exact) Jacobians associated with the problem are not required for the computation! Moreover, this flexibility enables us to implement the central scheme *without* dimensional splitting.

The motivation for our construction of the two-dimensional central scheme discussed in this paper originates with the one-dimensional central scheme introduced by Nessyahu and Tadmor in [NT]. To begin with, we briefly recall this one-dimensional setup. Starting with a piecewise-constant solution, $\sum \bar{w}_p^n \chi_p(x)$, one reconstructs a piecewise-linear approximation, $w(x, t^n) = \sum \left[\bar{w}_p^n + w_p' \left(\frac{x - x_p}{\Delta x} \right) \right] \chi_p(x)$. Here, $\chi_p(x)$ is a characteristic function of the cell, $I_p := \{\xi \, \big| \, |\xi - x_p| \leq \frac{\Delta x}{2}\}$, centered around $x_p = p\Delta x$, and w_p' abbreviates a first-order discrete slope which is reconstructed from the neighboring cell averages $\{\bar{w}_q^n\}$. Let $\{w(x, t), \ t \geq t^n\}$ be the exact solution of the conservation law $w_t + f(w)_x = 0$, subject to the *reconstructed* initial data at $t = t^n$; the distinctive feature of central schemes, in contrast to Godunov-type upwind schemes, is that they realize this exact solution by its averages over *staggered* cells, $I_{j+\frac{1}{2}}$, centered around $x_{j+\frac{1}{2}} = \left(j + \frac{1}{2} \right) \Delta x$. Let $\bar{w}_{j+\frac{1}{2}}(t) := \frac{1}{\Delta x} \int_{I_{j+\frac{1}{2}}} w(\xi, t)d\xi$ denote these staggered averages. Integration over the control volume $I_{j+\frac{1}{2}} \times [t^n, t^{n+1}]$ yields (with the usual fixed mesh-ratio $\lambda := \frac{\Delta t}{\Delta x}$)

$$\bar{w}_{j+\frac{1}{2}}(t^{n+1}) = \bar{w}_{j+\frac{1}{2}}(t^n) - \lambda \left[\frac{1}{\Delta t} \int_{t^n}^{t^{n+1}} f(w_{j+1}(\tau))d\tau - \frac{1}{\Delta t} \int_{t^n}^{t^{n+1}} f(w_j(\tau))d\tau \right].$$

The averaging of the piecewise-linear data reconstructed at $t = t^n$ yields $\bar{w}_{j+\frac{1}{2}}(t^n) = \frac{1}{2}(w_j^n + w_{j+1}^n) + \frac{1}{8}(w_j' - w_{j+1}')$. So far everything is *exact*. At this point the fluxes on

the right are *approximated* by the midpoint rule, $\frac{1}{\Delta t}\int_{t^n}^{t^{n+1}} f(w_j(\tau))d\tau \sim f(w_j(t^{n+\frac{1}{2}}))$. The Conrant–Friedrichs–Levy (CFL) condition guarantees that the interface values, $w_j(\tau) = w(x_j, \tau), \tau \in [t^n, t^{n+1})$, are "secured" within a smooth region, so one may use Taylor expansion to approximate the midvalue $w_j(t^{n+\frac{1}{2}})$. We end up with a predictor step for these midvalues,

$$(1.1) \qquad w_j^{n+\frac{1}{2}} = \bar{w}_j^n - \frac{\lambda}{2}(f(w_j))',$$

followed by the corrector step described above,

$$(1.2) \qquad \bar{w}_{j+\frac{1}{2}}^{n+1} = \frac{1}{2}(\bar{w}_j^n + \bar{w}_{j+1}^n) + \frac{1}{8}(w_j' - w_{j+1}') - \lambda\left[f(w_{j+1}^{n+\frac{1}{2}}) - f(w_j^{n+\frac{1}{2}})\right].$$

Here, w_j', and likewise, $f(w_j)'$, denote spatial *discrete slopes* of the corresponding grid functions. There is a variety of recipes for the construction of such slopes; see e.g., [Sw], [LO]. These discrete slopes involve nonlinear limiters, which guarantee that the central scheme (1.1)–(1.2) is nonoscillatory in the sense described below.

1.1. One-dimensional epilogue: No characteristic decompositions. The scalar central scheme (1.1)–(1.2) shares desirable nonoscillatory properties with the scalar high-resolution *upwind* schemes. In this context we refer to proofs of total variation bounds (the total variation diminishing (TVD) property [Ha2]), entropy stability (cell entropy inequality [OT]), maximum principle, etc.; consult [NT], [Hu], [LT]. The distinctive advantage of the central schemes, however, is due to their nonoscillatory behavior with *systems* of conservation laws. Specifically, the *vector* of discrete slopes required in the corrector step (1.2), w_j', is now implemented using a straightforward *componentwise* extension of the scalar recipes. In particular, for the discrete derivative of the flux in the predictor step (1.1), we may use $f(w_j)' = A(w_j)w_j'$; alternatively, we can proceed with a straightforward *componentwise* computation of $f(w_j)'$, which does not even require the Jacobian, $A = f_w$. In either case, intricate and time-consuming characteristic decompositions of upwind differencing are avoided; a straightforward componentwise approach will do for the central scheme (1.1)–(1.2).

These advantages of the central framework were already borne out in several related works, e.g., [AV], [BS], [Er], [Hu], [LT], [NT], [SW], [Sa2], [TW]. Here we provide one more simple demonstration of this point in the context of the one-dimensional, constant-coefficients test system proposed to us by Engquist and Osher [EO],

$$(1.3) \qquad u_t + (Au)_x = 0, \qquad A := \begin{pmatrix} 0 & 1 \\ 1 & 0 \end{pmatrix},$$

subject to discontinuous initial data (and periodic boundary conditions)

$$(1.4) \qquad \begin{aligned} u_1(x,0) &\equiv 1, \\ u_2(x,0) &= \begin{cases} 1, & x < 0, \\ 0, & x > 0. \end{cases} \end{aligned}$$

Careful numerical simulations are required to model the propagation of such initial singularities. Let us recall that postprocessing and artificial compression of contact discontinuities, e.g., [MO], [Ha1], are just two remedies to the spurious oscillations which are formed in connection with the numerical simulations of such singularities. Figure 1.1 compares the results of the central scheme (1.1)–(1.2) using the MinMod
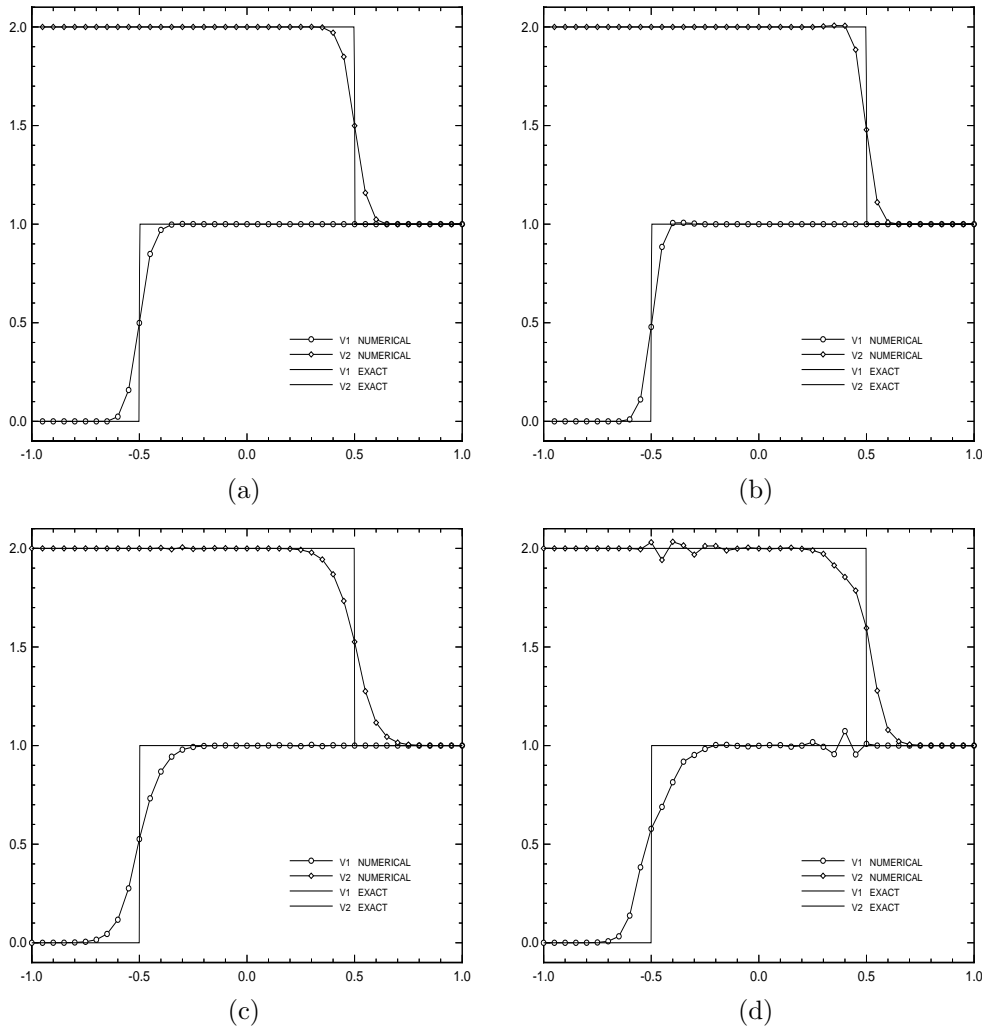
FIG. 1.1. The 2×2 system (1.3)–(1.4) evaluated with $N = 40$ cells and $CFL = 0.4$ at $t = 0.5$. Plotted are numerical and exact characteristic variables. Nessyahu–Tadmor scheme (1.1)–(1.2) with MinMod limiter in $(3.1')$: (a) with MM_1 limiter; (b) with MM_2 limiter. Results are compared with ENO-ROE scheme: (c) componentwise second-order ENO-ROE; (d) componentwise third-order ENO-ROE.

limiter MM_θ outlined in $(3.1')$, with those of the upwind ENO–ROE scheme outlined in [JS]. Both schemes used *componentwise* reconstructions of pointvalues from cell averages. Figures 1.1a,b demonstrate that the central scheme is able to perfectly resolve the discontinuities carried by each of the characteristic variables, $v_1 := u_1 + u_2$ and $v_2 := u_1 - u_2$, *without* spurious oscillations in the other characteristic variable. One can detect such oscillations, however, in the second-order upwind results of Figure 1.1c, oscillations which become more pronounced in the third-order results of Figure 1.1d. This type of behavior repeated itself in a variety of test cases we have tried with different systems and stronger jump amplitudes.

2. The two-dimensional central scheme.

2.1. A two-step predictor-corrector formulation. We consider the two-dimensional system of conservation laws

$$(2.1) \qquad u_t + f(u)_x + g(u)_y = 0,$$

subject to prescribed initial data, $u(x, y, t = 0) = u_0(x, y)$. To approximate (2.1) by a central scheme, we begin with a piecewise constant solution of the form $\sum \bar{w}^n_{pq} \chi_{pq}(x, y)$. Here, $\bar{w}^n_{pq}$ is the approximate cell average at $t = t^n$, associated with the cell $C_{pq} = I_p \times J_q$ centered around $(x_p = p\Delta x, y_q = q\Delta y)$, i.e.,

$$C_{pq} := \left\{ (\xi, \eta) \,\Big|\, |\xi - x_p| \le \frac{\Delta x}{2}, \ |\eta - y_q| \le \frac{\Delta y}{2} \right\}.$$

As a first step, we *reconstruct* a piecewise-linear approximation of the form

$$(2.2) \qquad w(x, y, t^n) = \sum \left[\bar{w}^n_{pq} + w'_{pq} \left(\frac{x - x_p}{\Delta x} \right) + w^{\backprime}_{pq} \left(\frac{y - y_q}{\Delta y} \right) \right] \chi_{pq}(x, y).$$

Here, w'_{pq} and $w^{\backprime}_{pq}$ are *discrete slopes* in the x- and y-directions, respectively, which are reconstructed from the given cell averages. To guarantee second-order accuracy, these slopes should approximate the corresponding derivatives,

$$(2.3') \qquad w'_{pq} \sim \Delta x \cdot w_x(x_p, y_q, t^n) + \mathcal{O}(\Delta x)^2,$$

$$(2.3^{\backprime}) \qquad w^{\backprime}_{pq} \sim \Delta y \cdot w_y(x_p, y_q, t^n) + \mathcal{O}(\Delta y)^2.$$

As in the one-dimensional framework, the construction of our central scheme proceeds with a second step of an exact evolution followed by staggered averaging.

Let $\{w(x, y, t), \ t \ge t^n\}$ be the exact solution of the conservation law (2.1),

$$(2.4) \qquad w_t + f(w)_x + g(w)_y = 0, \quad t \ge t^n,$$

subject to the reconstructed piecewise-linear data (2.2), $w(x, y, t^n)$, at $t = t^n$. The second (and distinctive) step is to realize this exact solution at the next time step $t = t^{n+1}$, by its averages over *staggered* cells, $C_{j+\frac{1}{2}, k+\frac{1}{2}} := I_{j+\frac{1}{2}} \times J_{k+\frac{1}{2}}$, centered around $(x_{j+\frac{1}{2}}, y_{k+\frac{1}{2}})$.

Let $\bar{w}_{j+\frac{1}{2}, k+\frac{1}{2}}(t) = \fint_{C_{j+\frac{1}{2}, k+\frac{1}{2}}} w(x, y, t) dx dy$ denote these staggered averages. (Here and below we abbreviate $\fint_B := \frac{1}{|B|} \int_B$ to denote the *normalized* integral—normalized over its length, area, etc.) Let $\lambda := \frac{\Delta t}{\Delta x}$ and $\mu := \frac{\Delta t}{\Delta y}$ denote the fixed mesh-ratios. Integration of (2.4) over $C_{j+\frac{1}{2}, k+\frac{1}{2}} \times [t^n, t^{n+1})$ yields
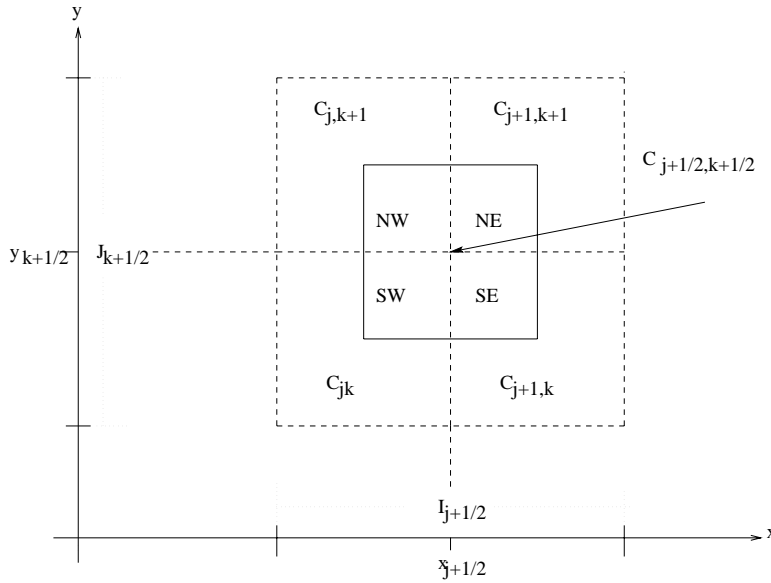
FIG. 2.1. *Floor plan of the staggered grid.*

$$\bar{w}_{j+\frac{1}{2},k+\frac{1}{2}}(t^{n+1}) = \fint_{C_{j+\frac{1}{2},k+\frac{1}{2}}} w(x,y,t^n)dxdy$$

$$- \lambda \left\{ \int_{\tau=t^n}^{t^{n+1}} \fint_{y \in J_{k+\frac{1}{2}}} [f(w(x_{j+1},y,\tau)) - f(w(x_j,y,\tau))] \, dyd\tau \right\}$$

(2.5)
$$- \mu \left\{ \int_{\tau=t^n}^{t^{n+1}} \fint_{x \in I_{j+\frac{1}{2}}} [g(w(x,y_{k+1},\tau)) - g(w(x,y_k,\tau))] \, dxd\tau \right\}.$$

We begin by evaluating the cell average, $\fint_{C_{j+\frac{1}{2},k+\frac{1}{2}}} w(x,y,t^n)dxdy$. It has contributions from the four intersecting cells, $C_{jk}, C_{j+1,k}, C_{j+1,k+1}$, and $C_{j,k+1}$. Starting with the intersecting cell C_{jk} at the southwest corner (consult Figure 2.1), $C^{SW}_{j+\frac{1}{2},k+\frac{1}{2}} :=$ $C_{j+\frac{1}{2},k+\frac{1}{2}} \cap C_{jk}$, we find the average of the reconstructed polynomial in (2.2),

$$\fint_{C^{SW}_{j+\frac{1}{2},k+\frac{1}{2}}} w(x,y,t^n)dxdy$$

$$= \fint_{x_j}^{x_{j+\frac{1}{2}}} \fint_{y_k}^{y_{k+\frac{1}{2}}} \left[\bar{w}^n_{jk} + w'_{jk} \left(\frac{x-x_j}{\Delta x} \right) + w\grave{}_{jk} \left(\frac{y-y_k}{\Delta y} \right) \right] dxdy$$

(2.6)
$$= \frac{1}{4} \bar{w}^n_{jk} + \frac{1}{16} (w'_{jk} + w\grave{}_{jk}).$$

Continuing in a counterclockwise direction, we have

$$(2.7) \qquad \fint_{C^{SE}_{j+\frac{1}{2},k+\frac{1}{2}}} w(x,y,t^n)dxdy = \frac{1}{4}\bar{w}^n_{j+1,k} + \frac{1}{16}(-w'_{j+1,k} + w\grave{}_{j+1,k}),$$

$$(2.8) \qquad \fint_{C^{NE}_{j+\frac{1}{2},k+\frac{1}{2}}} w(x,y,t^n)dxdy = \frac{1}{4}\bar{w}^n_{j+1,k+1} - \frac{1}{16}\left(w'_{j+1,k+1} + w\grave{}_{j+1,k+1}\right),$$

$$(2.9) \qquad \fint_{C^{NW}_{j+\frac{1}{2},k+\frac{1}{2}}} w(x,y,t^n)dxdy = \frac{1}{4}\bar{w}^n_{j,k+1} + \frac{1}{16}\left(w'_{j,k+1} - w\grave{}_{j,k+1}\right).$$

By adding the last four integrals we find the exact staggered averages of the reconstructed solution at $t = t^n$,

$$(2.10)$$

$$\bar{w}^n_{j+\frac{1}{2},k+\frac{1}{2}} := \fint_{C_{j+\frac{1}{2},k+\frac{1}{2}}} w(x,y,t^n)dxdy$$

$$= \frac{1}{4}(\bar{w}^n_{jk} + \bar{w}^n_{j+1,k} + \bar{w}^n_{j,k+1} + \bar{w}^n_{j+1,k+1})$$

$$+ \frac{1}{16}\Big\{(w'_{jk} - w'_{j+1,k}) + (w'_{j,k+1} - w'_{j+1,k+1})$$

$$+ (w\grave{}_{jk} - w\grave{}_{j,k+1}) + (w\grave{}_{j+1,k} - w\grave{}_{j+1,k+1})\Big\}.$$

So far everything is *exact*. We now turn to *approximating* the four fluxes on the right of (2.5), starting with the one along the east face (consult Figure 2.2), $\fint_{t^n}^{t^{n+1}} \fint_{J_{k+\frac{1}{2}}} f(w(x_{j+1},y,\tau))dyd\tau$. We use the midpoint quadrature rule for second-order approximation of the temporal integral, $\fint_{y\in J_{k+\frac{1}{2}}} f(w(x_{j+1},y,t^{n+\frac{1}{2}}))dy$; and, for reasons to be clarified below, we use the second-order rectangular quadrature rule for the spatial integration across the y-axis, yielding

$$(2.11) \qquad \fint_{t^n}^{t^{n+1}} \fint_{y\in J_{k+\frac{1}{2}}} f(w(x_{j+1},y,\tau))dyd\tau \sim \frac{1}{2}\left[f(w^{n+\frac{1}{2}}_{j+1,k}) + f(w^{n+\frac{1}{2}}_{j+1,k+1})\right].$$

In a similar manner we approximate the remaining fluxes,

$$(2.12) \qquad \fint_{t^n}^{t^{n+1}} \fint_{x\in I_{j+\frac{1}{2}}} g(w(x,y_{k+1},\tau))dxd\tau \sim \frac{1}{2}\left[g(w^{n+\frac{1}{2}}_{j,k+1}) + g(w^{n+\frac{1}{2}}_{j+1,k+1})\right],$$

$$(2.13) \qquad \fint_{t^n}^{t^{n+1}} \fint_{y\in J_{k+\frac{1}{2}}} f(w(x_j,y,\tau))dyd\tau \sim \frac{1}{2}\left[f(w^{n+\frac{1}{2}}_{jk}) + f(w^{n+\frac{1}{2}}_{j,k+1})\right],$$

$$(2.14) \qquad \fint_{t^n}^{t^{n+1}} \fint_{x\in I_{j+\frac{1}{2}}} g(w(x,y_k,\tau))dxd\tau \sim \frac{1}{2}\left[g(w^{n+\frac{1}{2}}_{jk}) + g(w^{n+\frac{1}{2}}_{j+1,k})\right].$$

The approximate fluxes in (2.11)–(2.14) make use of the midpoint values, $w^{n+\frac{1}{2}}_{jk} \equiv w(x_j,y_k,t^{n+\frac{1}{2}})$, and it is here that we take advantage of utilizing these midvalues for the spatial integration by the rectangular rule. Namely, since these midvalues
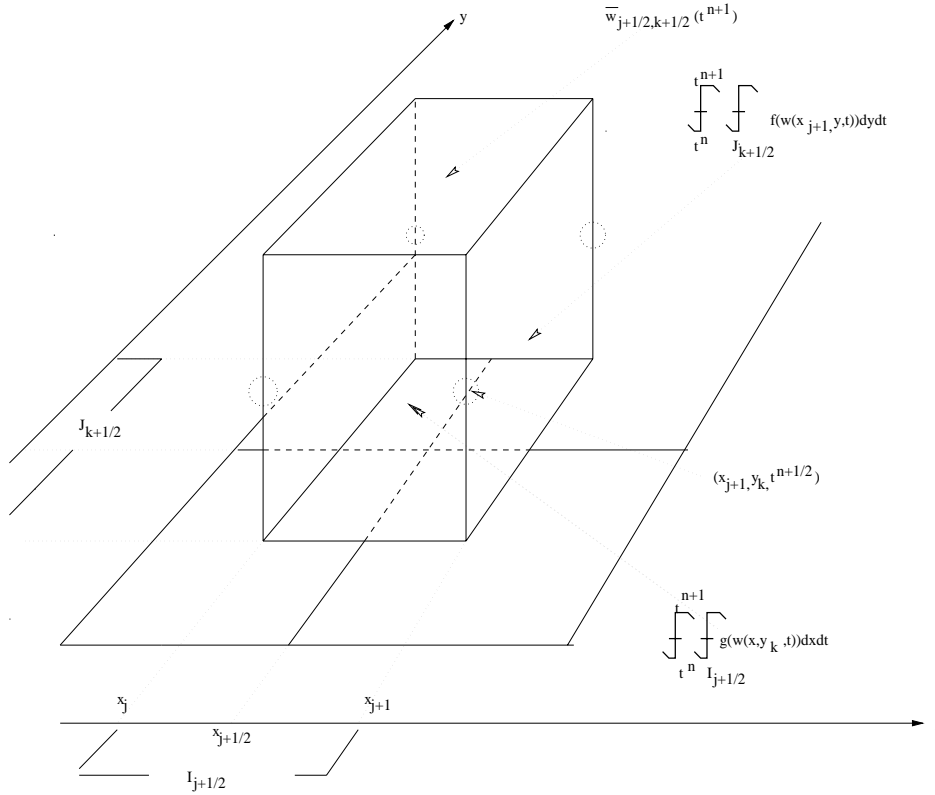
FIG. 2.2. *The central, staggered stencil.*

are secured at the smooth center of their cells, C_{jk}, bounded away from the jump discontinuities along the edges, we may use Taylor expansion, $w(x_j, y_k, t^{n+\frac{1}{2}}) = \bar{w}_{jk}^n + \frac{\Delta t}{2} w_t(x_j, y_k, t^n) + \mathcal{O}(\Delta t)^2$. Finally, we use the conservation law (2.4) to express the time derivative, w_t, in terms of the spatial derivatives, $f(w)'$ and $g(w)^\backslash$,

$$(2.15) \qquad w_{jk}^{n+\frac{1}{2}} = \bar{w}_{jk}^n - \frac{\lambda}{2} f(w)'_{jk} - \frac{\mu}{2} g(w)^\backslash_{jk}.$$

Here, $f(w)'_{jk} \sim \Delta x \cdot f(w(x_j, y_k, t^n))_x$ and $g(w)^\backslash_{jk} \sim \Delta y \cdot g(w(x_j, y_k, t^n))_y$ are one-dimensional discrete slopes in the x- and y-directions, of the type reconstructed in (2.3′); for example, multiplication of (2.3′)–(2.3$^\backslash$) by the corresponding Jacobians A and B yields

$$f(w)'_{jk} = A(\bar{w}_{jk}^n) w'_{jk}, \qquad g(w)^\backslash_{jk} = B(\bar{w}_{jk}^n) w^\backslash_{jk}.$$

Equipped with the midvalues (2.15), we can now evaluate the approximate fluxes (2.11)–(2.14). Inserting these values, together with the staggered average computed in (2.11), into (2.5), we conclude with new staggered averages at $t = t^{n+1}$, given by

$$(2.16) \quad \bar{w}_{j+\frac{1}{2}, k+\frac{1}{2}}^{n+1} = \frac{1}{4}(\bar{w}_{jk}^n + \bar{w}_{j+1,k}^n + \bar{w}_{j,k+1}^n + \bar{w}_{j+1,k+1}^n)$$
$$+ \frac{1}{16}(w'_{jk} - w'_{j+1,k}) - \frac{\lambda}{2}\left[f(w_{j+1,k}^{n+\frac{1}{2}}) - f(w_{j,k}^{n+\frac{1}{2}})\right]$$

$$+ \frac{1}{16}(w'_{j,k+1} - w'_{j+1,k+1}) - \frac{\lambda}{2}\left[f(w^{n+\frac{1}{2}}_{j+1,k+1}) - f(w^{n+\frac{1}{2}}_{j,k+1}) \right]$$
$$+ \frac{1}{16}(w^{\backslash}_{jk} - w^{\backslash}_{j,k+1}) - \frac{\mu}{2}\left[g(w^{n+\frac{1}{2}}_{j,k+1}) - g(w^{n+\frac{1}{2}}_{j,k}) \right]$$
$$+ \frac{1}{16}(w^{\backslash}_{j+1,k} - w^{\backslash}_{j+1,k+1}) - \frac{\mu}{2}\left[g(w^{n+\frac{1}{2}}_{j+1,k+1}) - g(w^{n+\frac{1}{2}}_{j+1,k}) \right].$$

In summary, we end up with a simple two-step predictor-corrector scheme (2.15)–(2.16). Starting with the cell averages, $\bar{w}^n_{jk}$, we use the first-order predictor (2.15) for the evaluation of the midpoint values, $w^{n+\frac{1}{2}}_{jk}$, which is followed by the second-order corrector (2.16) for the computation of the new cell averages, $\bar{w}^{n+1}_{jk}$. This results in a second-order accurate nonoscillatory scheme. As in the one-dimensional case—no (approximate) Riemann solvers are involved—the nonoscillatory behavior of the scheme hinges on the reconstructed discrete slopes, w', $w^{\backslash}$, $f(w)'$, and $g(w)^{\backslash}$.

2.2. A one-dimensional-like formulation revisited. The corrector step (2.16) bears a close similarity with the one-dimensional corrector formula (1.2). Indeed, let us introduce the notation for staggered averaging in the x- and y-directions,

$$\langle \omega_{j,\cdot} \rangle_{k+\frac{1}{2}} := \frac{1}{2}(\omega_{jk} + \omega_{j,k+1}), \quad \langle \omega_{\cdot,k} \rangle_{j+\frac{1}{2}} := \frac{1}{2}(\omega_{jk} + \omega_{j+1,k}).$$

Then (2.16) takes the simple one-dimensional-like form (compare the one-dimensional corrector in (1.2))

$$\bar{w}^{n+1}_{j+\frac{1}{2},k+\frac{1}{2}} = \left\langle \frac{1}{4}(\bar{w}^n_{j,\cdot} + \bar{w}^n_{j+1,\cdot}) + \frac{1}{8}(w'_{j,\cdot} - w'_{j+1,\cdot}) - \lambda[f(w^{n+\frac{1}{2}}_{j+1,\cdot}) - f(w^{n+\frac{1}{2}}_{j,\cdot})] \right\rangle_{k+\frac{1}{2}}$$
$$+ \left\langle \frac{1}{4}(\bar{w}^n_{\cdot,k} + \bar{w}^n_{\cdot,k+1}) + \frac{1}{8}(w^{\backslash}_{\cdot,k} - w^{\backslash}_{\cdot,k+1}) - \mu[g(w^{n+\frac{1}{2}}_{\cdot,k+1}) - g(w^{n+\frac{1}{2}}_{\cdot,k})] \right\rangle_{j+\frac{1}{2}}.$$

3. The maximum principle for scalar approximations. It is well known that the exact entropy solution of the *scalar* conservation law (2.1) satisfies a maximum principle. In this section we prove that under an appropriate CFL condition, our central scheme (2.15)–(2.16) satisfies the same maximum principle. To this end, it is essential to reconstruct the discrete slopes, w' and $w^{\backslash}$, with built-in *limiters*, which we now briefly describe in the context of the prototype example

$$(3.1') \quad w'_{jk} = MM\left\{ \theta(\bar{w}^n_{j+1,k} - \bar{w}^n_{j,k}), \frac{1}{2}(\bar{w}^n_{j+1,k} - \bar{w}^n_{j-1,k}), \theta(\bar{w}^n_{j,k} - \bar{w}^n_{j-1,k}) \right\},$$

$$(3.1^{\backslash}) \quad w^{\backslash}_{jk} = MM\left\{ \theta(\bar{w}^n_{j,k+1} - \bar{w}^n_{j,k}), \frac{1}{2}(\bar{w}^n_{j,k+1} - \bar{w}^n_{j,k-1}), \theta(\bar{w}^n_{j,k} - \bar{w}^n_{j,k-1}) \right\}.$$

Here, the choice $\theta = 1$ coincides with the "classical" so-called MinMod limiter, e.g., [Ha1], [Sw]; it guarantees that the corresponding piecewise-linear reconstruction in (2.2), $w(x, y, t^n)$, is *co-monotone* with the underlying piecewise-constant approximation, $\sum \bar{w}^n_{pq}\chi_{pq}$. The range of θ's, $1 \leq \theta \leq 2$, allows for a further variety of accurate reconstructions which satisfy the maximum principle, $\|w(\cdot, t^n)\|_{L^\infty} \leq \|\sum \bar{w}^n_{pq}\chi_{pq}(\cdot)\|_{L^\infty}$. The essential feature in the definition of these discrete slopes, however, is due to the MinMod function: its output equals the input variable with

minimal modules among all its input variables, unless the latter disagree in sign, in which case $MM = 0$,

$$MM\{v_1, v_2, \ldots\} = \begin{cases} \min_p \{v_p\} & \text{if } v_p > 0 \; \forall p, \\ \max_p \{v_p\} & \text{if } v_p < 0 \; \forall p, \\ 0 & \text{otherwise.} \end{cases}$$

In particular, the so-called *clipping phenomena* may occur, due to the reconstruction of zero discrete slopes at extrema cells (where forward and backward differences change signs). The clipping limiter feature is clearly necessary to retain the maximum principle at the reconstruction step. It implies that the neighboring discrete slopes cannot have *opposite* signs, and in particular,

(3.2) $\quad |w'_{j+1,k} - w'_{j,k}| \leq \max(|w'_{j+1,k}|, |w'_{j,k}|) \leq \theta |\bar{w}_{j+1,k} - \bar{w}_{j,k}|, \quad 1 \leq \theta < 2,$

(3.3) $\quad |w^\backprime_{j,k+1} - w^\backprime_{j,k}| \leq \max(|w^\backprime_{j,k+1}|, |w^\backprime_{j,k}|) \leq \theta |\bar{w}_{j,k+1} - \bar{w}_{j,k}|, \quad 1 \leq \theta < 2.$

Similar estimates apply to the reconstructed discrete slopes for the flux; for example,

(3.4) $\quad |f(w)'_{j+1,k} - f(w)'_{jk}| \leq \max(|f(w)'_{j+1,k}|, |f(w)'_{jk}|) \leq \theta |f(\bar{w}^n_{j+1,k}) - f(\bar{w}^n_{jk})|.$

THEOREM 1. *Consider the two-dimensional scalar scheme* (2.15)–(2.16). *Assume that the discrete slopes, w' and $w^\backprime$, satisfy the (θ-dependent) limiter property* (3.2)–(3.3), *and likewise for $f(w)'$ and $g(w)^\backprime$ (e.g., the MinMod limiter* (3.1')–(3.1^\backprime)). *Then for any $\theta < 2$ there exists a sufficiently small CFL number, C_θ (e.g., $C_1 = (\sqrt{7} - 2)/6 \sim 0.1$), such that if the CFL condition is fulfilled,*

$$\max(\lambda \cdot \max_u |f_u(u)|, \mu \cdot \max_u |g_u(u)|) \leq C_\theta,$$

then the following local maximum principle holds:

(3.5) $$\min_{\substack{|p-(j+\frac{1}{2})|=\frac{1}{2} \\ |q-(k+\frac{1}{2})|=\frac{1}{2}}} \{\bar{w}^n_{p,q}\} \leq \bar{w}^{n+1}_{j+\frac{1}{2},k+\frac{1}{2}} \leq \max_{\substack{|p-(j+\frac{1}{2})|=\frac{1}{2} \\ |q-(k+\frac{1}{2})|=\frac{1}{2}}} \{\bar{w}^n_{p,q}\}.$$

Proof. Our key observation is to rewrite the new value computed in (2.16), $\bar{w}^{n+1}_{j+\frac{1}{2},k+\frac{1}{2}}$, as the average of four distinctive terms,

$$\bar{w}^{n+1}_{j+\frac{1}{2},k+\frac{1}{2}} = \frac{1}{4}$$

$$\times \left\{ \frac{1}{2}\left(\bar{w}^n_{jk} + \bar{w}^n_{j+1,k}\right) + \frac{1}{4}\left(w'_{jk} - w'_{j+1,k}\right) - 2\lambda\left(f^{n+\frac{1}{2}}_{j+1,k} - f^{n+\frac{1}{2}}_{j,k}\right) \right.$$

$$+ \frac{1}{2}\left(\bar{w}^n_{j,k+1} + \bar{w}^n_{j+1,k+1}\right) + \frac{1}{4}\left(w'_{j,k+1} - w'_{j+1,k+1}\right) - 2\lambda\left(f^{n+\frac{1}{2}}_{j+1,k+1} - f^{n+\frac{1}{2}}_{j,k+1}\right)$$

(3.6) $$+ \frac{1}{2}\left(\bar{w}^n_{jk} + \bar{w}^n_{j,k+1}\right) + \frac{1}{4}\left(w^\backprime_{jk} - w^\backprime_{j,k+1}\right) - 2\mu\left(g^{n+\frac{1}{2}}_{j,k+1} - g^{n+\frac{1}{2}}_{jk}\right)$$

$$\left. + \frac{1}{2}\left(\bar{w}^n_{j+1,k} + \bar{w}^n_{j+1,k+1}\right) + \frac{1}{4}\left(w^\backprime_{j+1,k} - w^\backprime_{j+1,k+1}\right) - 2\mu\left(g^{n+\frac{1}{2}}_{j+1,k+1} - g^{n+\frac{1}{2}}_{j+1,k}\right) \right\}$$

$$=: \frac{1}{4} \times \{\mathcal{I}_1 + \mathcal{I}_2 + \mathcal{I}_3 + \mathcal{I}_4\}.$$

Here and below we abbreviate $f^{n+\frac{1}{2}}_{jk} = f(\bar{w}^{n+\frac{1}{2}}_{jk})$.

We will show that each of these four terms, $\mathcal{I}_j$, can be written as an appropriate sum of the cell averages at t^n, $\{\bar{w}_{jk}^n, \bar{w}_{j+1,k}^n, \bar{w}_{j,k+1}^n, \bar{w}_{j+1,k+1}^n\}$, so that $\bar{w}_{j+\frac{1}{2},k+\frac{1}{2}}^{n+1}$ can be expressed as a *convex* combination of these averages. This implies, in particular, that the local maximum principle (3.5) holds.

We begin by estimating the difference between two neighboring midvalues, say $w_{j+1,k}^{n+\frac{1}{2}} - w_{jk}^{n+\frac{1}{2}}$, evaluated in the predictor step (2.15)

$$(3.7) \qquad w_{j+1,k}^{n+\frac{1}{2}} - w_{jk}^{n+\frac{1}{2}} = \bar{w}_{j+1,k}^n - \bar{w}_{jk}^n$$
$$- \frac{\lambda}{2}[f(w)_{j+1,k}' - f(w)_{jk}'] - \frac{\mu}{2}[g(w)_{j+1,k}^{\backslash} - g(w)_{jk}^{\backslash}].$$

Since by (3.4), $f(w)_{j+1,k}'$ and $f(w)_{jk}'$ cannot have opposite signs, their differences on the right of (3.7) do not exceed

$$(3.8) \qquad |f(w)_{j+1,k}' - f(w)_{jk}'| \leq \theta|f(\bar{w}_{j+1,k}^n) - f(\bar{w}_{jk}^n)| \leq \theta\mathsf{a}|\bar{w}_{j+1,k}^n - \bar{w}_{jk}^n|.$$

Here and below, $\mathsf{a} := \max_u|f_u(u)|$ and $\mathsf{b} := \max_u|g_u(u)|$ denote the maximal speeds in the x- and y-directions. The third difference on the right of (3.7), $g(w)_{j+1,k}^{\backslash} - g(w)_{jk}^{\backslash}$, represents a "mixed" derivative (which allows for opposite signs); here we use the straightforward (3.1'):

$$(3.9) \quad |g(w)_{j+1,k}^{\backslash} - g(w)_{jk}^{\backslash}| \leq |g(w)_{j+1,k}^{\backslash}| + |g(w)_{jk}^{\backslash}|$$
$$\leq \theta\left[|g(\bar{w}_{j+1,k+1}^n) - g(\bar{w}_{j+1,k}^n)| + |g(\bar{w}_{j,k+1}^n) - g(\bar{w}_{jk}^n)|\right]$$
$$\leq \theta\mathsf{b}\left[|\bar{w}_{j,k+1}^n - \bar{w}_{jk}^n| + |\bar{w}_{j+1,k+1}^n - \bar{w}_{j+1,k}^n|\right].$$

Using (3.8) and (3.9) we obtain an upper bound on the midvalues difference in (3.7), which in turn enables us to upperbound the corresponding flux difference

$$(3.10) \quad \lambda|f_{j+1,k}^{n+\frac{1}{2}} - f_{jk}^{n+\frac{1}{2}}| \leq \lambda\mathsf{a}|w_{j+1,k}^{n+\frac{1}{2}} - w_{jk}^{n+\frac{1}{2}}|$$
$$\leq \frac{1}{2}\lambda\mathsf{a}(2 + \theta \cdot \lambda\mathsf{a})|\bar{w}_{j+1,k}^n - \bar{w}_{jk}^n|$$
$$+ \frac{1}{2}\theta \cdot \lambda\mathsf{a} \cdot \mu\mathsf{b}\left[|\bar{w}_{j,k+1}^n - \bar{w}_{jk}^n| + |\bar{w}_{j+1,k+1}^n - \bar{w}_{j+1,k}^n|\right].$$

We now return to the first term, $\mathcal{I}_1$, in (3.6): by (3.2) and (3.10), it does not exceed

$$\mathcal{I}_1 \leq \frac{1}{2}(\bar{w}_{jk}^n + \bar{w}_{j+1,k}^n) + \left(\frac{\theta}{4} + \lambda\mathsf{a}(2 + \theta \cdot \lambda\mathsf{a})\right)|\bar{w}_{j+1,k}^n - \bar{w}_{jk}^n|$$
$$+ \theta \cdot \lambda\mathsf{a} \cdot \mu\mathsf{b}|\bar{w}_{j,k+1}^n - \bar{w}_{jk}^n| + \theta \cdot \lambda\mathsf{a} \cdot \mu\mathsf{b}|\bar{w}_{j+1,k+1}^n - \bar{w}_{j+1,k}^n|.$$

Thus

$$(3.11) \qquad \mathcal{I}_1 \leq \mathcal{I}_{11} + \mathcal{I}_{12} + \mathcal{I}_{13} + \mathcal{I}_{14},$$

where

$$\mathcal{I}_{11} = \frac{1}{2}(\bar{w}_{jk}^n + \bar{w}_{j+1,k}^n), \quad \mathcal{I}_{12} = \alpha_{\lambda\mathsf{a}}|\bar{w}_{j+1,k}^n - \bar{w}_{jk}^n|, \qquad \alpha_{\lambda\mathsf{a}} := \frac{\theta}{4} + \lambda\mathsf{a}(2 + \theta \cdot \lambda\mathsf{a}),$$
$$\mathcal{I}_{13} = \beta|\bar{w}_{j,k+1}^n - \bar{w}_{jk}^n|, \quad \mathcal{I}_{14} = \beta|\bar{w}_{j+1,k+1}^n - \bar{w}_{j+1,k}^n|, \quad \beta := \theta \cdot \lambda\mathsf{a} \cdot \mu\mathsf{b}.$$

In a similar manner we obtain

$$(3.12) \quad \mathcal{I}_2 \leq \frac{1}{2}(\bar{w}_{j,k+1}^n + \bar{w}_{j+1,k+1}^n) + \alpha_{\lambda\mathsf{a}}|\bar{w}_{j+1,k+1}^n - \bar{w}_{j,k+1}^n|$$
$$+ \beta|\bar{w}_{j,k+1}^n - \bar{w}_{jk}^n| + \beta|\bar{w}_{j+1,k+1}^n - \bar{w}_{j+1,k}^n| =: \mathcal{I}_{21} + \mathcal{I}_{22} + \mathcal{I}_{23} + \mathcal{I}_{24};$$

$$(3.13) \quad |\mathcal{I}_3| \leq \frac{1}{2}(w_{jk}^n + \bar{w}_{j,k+1}^n) + \alpha_{\mu\mathsf{b}}|\bar{w}_{j,k+1}^n - \bar{w}_{jk}^n|$$
$$+ \beta|\bar{w}_{j+1,k}^n - \bar{w}_{jk}^n| + \beta|\bar{w}_{j+1,k+1}^n - \bar{w}_{j,k+1}^n| =: \mathcal{I}_{31} + \mathcal{I}_{32} + \mathcal{I}_{33} + \mathcal{I}_{34},$$

and finally

$$(3.14) \quad |\mathcal{I}_4| \leq \frac{1}{2}(\bar{w}_{j+1,k}^n + \bar{w}_{j+1,k+1}^n) + \alpha_{\mu\mathsf{b}}|\bar{w}_{j+1,k+1}^n - \bar{w}_{j+1,k}^n|$$
$$+ \beta|\bar{w}_{j+1,k}^n - \bar{w}_{j,k}^n| + \beta|\bar{w}_{j+1,k+1}^n - \bar{w}_{j,k+1}^n| =: \mathcal{I}_{41} + \mathcal{I}_{42} + \mathcal{I}_{43} + \mathcal{I}_{44}.$$

We now conclude by regrouping similar terms in the last four bounds; specifically, we rearrange the summation of the last four bounds in (3.11)–(3.14),

$$\sum_{j=1}^{4} \mathcal{I}_j = (\mathcal{I}_{11} + \mathcal{I}_{12} + \mathcal{I}_{33} + \mathcal{I}_{43}) + (\mathcal{I}_{21} + \mathcal{I}_{22} + \mathcal{I}_{34} + \mathcal{I}_{44}) + \cdots,$$

and we obtain

$$\bar{w}_{j+\frac{1}{2},k+\frac{1}{2}}^{n+1} = \frac{1}{4}\sum_{j=1}^{4}\mathcal{I}_j \leq \frac{1}{4}$$
$$\times \left\{ \frac{1}{2}(\bar{w}_{jk}^n + \bar{w}_{j+1,k}^n) + (\alpha_{\lambda\mathsf{a}} + 2\beta)|\bar{w}_{j+1,k}^n - \bar{w}_{jk}^n| \right.$$
$$+ \frac{1}{2}(\bar{w}_{j,k+1}^n + \bar{w}_{j+1,k+1}^n) + (\alpha_{\lambda\mathsf{a}} + 2\beta)|\bar{w}_{j+1,k+1}^n - \bar{w}_{j,k+1}^n|$$
$$+ \frac{1}{2}(\bar{w}_{jk}^n + \bar{w}_{j,k+1}^n) + (\alpha_{\mu\mathsf{b}} + 2\beta)|\bar{w}_{j,k+1}^n - \bar{w}_{jk}^n|$$
$$\left. + \frac{1}{2}(\bar{w}_{j+1,k}^n + \bar{w}_{j+1,k+1}^n) + (\alpha_{\mu\mathsf{b}} + 2\beta)|\bar{w}_{j+1,k+1}^n - \bar{w}_{j+1,k}^n| \right\}.$$

Our assertion concerning the convex combination, and hence the local maximum principle, follows, provided the following inequalities hold:

$$(3.15) \qquad\qquad \alpha_{\lambda\mathsf{a}} + 2\beta \equiv \frac{\theta}{4} + \lambda\mathsf{a}\left(2 + \theta \cdot \lambda\mathsf{a} + 2\theta \cdot \mu\mathsf{b}\right) \leq \frac{1}{2},$$

$$(3.16) \qquad\qquad \alpha_{\mu\mathsf{b}} + 2\beta \equiv \frac{\theta}{4} + \mu\mathsf{b}\left(2 + \theta \cdot \mu\mathsf{b} + 2\theta \cdot \lambda\mathsf{a}\right) \leq \frac{1}{2}.$$

Clearly, for any $\theta < 2$, these inequalities are satisfied for a sufficiently small CFL number, $\lambda\mathsf{a} + \mu\mathsf{b}$. For example, for the "canonical" MinMod limiter (with $\theta = 1$), we find that (3.15)–(3.16) hold provided $\max(\lambda\mathsf{a}, \mu\mathsf{b})$ does not exceed the largest root of $12\kappa^2 + 8\kappa - 1 = 0$, which yields (3.5).

4. Numerical experiments. Two-dimensional high resolution.

4.1. Scalar numerical results. Theorem 1 does not indicate the optimal CFL limitation. By measuring the wave propagation of the two-dimensional Riemann fan from the cell center at $(x_{j+\frac{1}{2}}, y_{k+\frac{1}{2}}, t^n)$ into the boundaries of that cell (consult Figure 1.1), we find the more realistic geometric CFL restriction $\max(\lambda\mathsf{a}, \mu\mathsf{b}) \leq \frac{1}{2}$. This is

TABLE 4.1
Second-order central approximation of $u_t + u_x + u_y = 0$ subject to $u_0(x, y) = \sin(\pi(x + y))$.

Limiter	N	L^∞ error	L^∞ order	L^1 error	L^1 order
			$CFL = 0.200$		
	40	4.91e-2	-	1.93e-2	-
MM_1	80	2.12e-2	1.21	5.70e-3	1.76
	160	8.90e-3	1.25	1.55e-3	1.88
	320	3.70e-3	1.27	4.14e-4	1.90
	40	1.06e-2	-	6.79e-3	-
MM_2	80	2.73e-3	1.96	1.81e-3	1.91
	160	6.86e-4	1.99	4.66e-4	1.96
	320	2.35e-4	1.55	1.17e-4	1.99
	40	1.08e-2	-	6.89e-3	-
UNO	80	2.73e-3	1.98	1.74e-3	1.99
	160	6.86e-4	1.99	4.37e-4	1.99
	320	1.72e-4	2.00	1.09e-4	2.00
			$CFL = 0.475$		
	40	4.53e-2	-	1.18e-2	-
MM_1	80	2.48e-2	0.87	6.40e-3	0.88
	160	1.92e-2	0.37	4.33e-3	0.56
	320	1.26e-1	-2.71	1.49e-2	-1.78
	40	1.34e-2	-	5.83e-3	-
MM_2	80	4.82e-3	1.48	1.74e-3	1.74
	160	1.41e-3	1.77	4.16e-4	2.06
	320	5.07e-4	1.48	1.29e-4	1.69
	40	9.08e-3	-	5.80e-3	-
UNO	80	2.74e-3	1.73	1.74e-3	1.74
	160	6.46e-4	2.08	4.11e-4	2.08
	320	1.48e-4	2.16	9.41e-5	2.13

confirmed by the results quoted in Table 4.1, where we record the test results with simple *linear oblique advection*, $u_t + u_x + u_y = 0$.

Here and below, we report the numerical results of the central scheme (2.15)–(2.16) with the MM_θ limiters in (3.1')–(3.1'); both $\theta = 1$ and $\theta = 2$ were used. We also tested the Harten–Osher UNO limiter [HO]

$$w'_{jk} = MM\left\{\Delta\bar{w}^n_{j-\frac{1}{2},k} + \frac{1}{2}MM(\Delta^2\bar{w}^n_{j-1,k}, \Delta^2\bar{w}^n_{jk}), \Delta\bar{w}^n_{j+\frac{1}{2},k} - \frac{1}{2}MM(\Delta^2\bar{w}^n_{jk}, \Delta^2\bar{w}^n_{j+1,k})\right\}.$$
(4.1)

Second-order accuracy, measured in L^1- and L^∞-norms, is detected for both CFLs 0.2 and .475. As expected, the second-order accuracy with the MinMod limiters MM_1 and MM_2 deteriorated due to the clipping phenomena. The fully second-order UNO limiter, however, retains the full L^1 second-order accuracy.

Next we turn to the two-dimensional *Burgers equation*:

$$\text{(4.2)} \qquad u_t + \frac{1}{2}(u^2)_x + \frac{1}{2}(u^2)_y = 0,$$

subject to "oblique" initial data,

$$u_0(x, y) = \begin{cases} -1.0, & x > 0, y > 0, \\ -0.2, & x < 0, y > 0, \\ 0.5, & x < 0, y < 0, \\ 0.8, & x > 0, y < 0. \end{cases}$$

The nonoscillatory behavior of the computed solution with CFL = .475 is demonstrated in Figure 4.1. In particular, no spurious oscillations are formed, in agreement with the maximum principle proved in section 3.

4.2. Efficiency and high resolution with hyperbolic systems. The proposed central scheme based on the predictor-corrector steps (2.15)–(2.16) offers a simple and robust *general-purpose* approximation for two-dimensional *systems* of hyperbolic conservation laws. In this subsection we highlight these advantages in the context of three prototype numerical experiments, governed by the two-dimensional Euler equations

$$(4.3) \qquad \begin{pmatrix} \rho \\ \rho u \\ \rho v \\ E \end{pmatrix}_t + \begin{pmatrix} \rho u \\ \rho u^2 + p \\ \rho u v \\ u(E + p) \end{pmatrix}_x + \begin{pmatrix} \rho v \\ \rho u v \\ \rho v^2 + p \\ v(E + p) \end{pmatrix}_y = 0,$$

expressed in terms of the usual density ρ, x- and y-velocities u and v, total energy E, and pressure $p := (\gamma - 1)(E - \frac{1}{2}\rho(u^2 + v^2))$.

For the reader's convenience, we enclose an Appendix with our central scheme code for the two-dimensional Euler system (4.3): the user supplies the number and size of spatial cells, the CFL number, the numerical solution at initial time $t = 0$, and the choice of a limiter: MM_θ, UNO, etc. (The code contains self-explanatory comments.) The code then evolves this solution up to the final time, t_f, using a two time-step cycle: regular cell $\longrightarrow$ staggered cell $\longrightarrow$ regular cell. For simplicity, the code is complemented with periodic boundary conditions in both x- and y-directions.

We begin with the *oblique Sod's problem*. Here we test the capability of our central scheme to resolve waves which are *oblique* to the computational domain. Following [JS] we initiate the two-dimensional Euler equations (4.3), with the standard one-dimensional Sod's Riemann data [So], whose initial jump discontinuity located at $(x, y) = (2.25, 0)$ was rotated to make an angle ϕ with the x-axis; consult [JS, section 8.3] for details. Figure 4.2 shows that the density at $t = 1.2$ is well resolved by the central scheme based on a computational grid of 192×32 cells and CFL $= 0.475$. Figure 4.3 compares the fully two-dimensional computation vs. the rotated results of the one-dimensional one; thus, the errors are "purely" due to the oblique nature of the computational waves. As is [JS], the deviations are negligible.

Our next example is the *double Mach reflection* problem [WC]. The two-dimensional Euler equations (4.3) are initiated with a right-moving Mach 10 shock positioned at $(x, y) = (1/6, 0)$, and makes a 60° angle with the x-axis.[1] The computational domain consists of the box $[0, 4] \times [0, 1]$. Boundary conditions: the bottom boundary consists of the exact postshock conditions at $[0, 1/6]$ followed by reflective boundary conditions for the rest; at the top boundary, the flow values are set to describe the exact motion of the Mach 10 shock. We refer to [WC] for a detailed description of this problem.

Figures 4.4–4.6 show the numerical results of the central scheme (2.15)–(2.16), using the MinMod and UNO limiters. *It is remarkable that such a simple "two-lines" algorithm, with no characteristic decompositions and no dimensional splitting, approximates the rather complicated double Mach reflection problem with such high resolution.* This should be compared, for example, with the higher (fourth and fifth orders) (W)ENO schemes in [JS, section 8.3]. A couple of remarks are in order.

---

[1] For simplicity, the initial cell averages were taken as the initial pointvalues at the midcells.
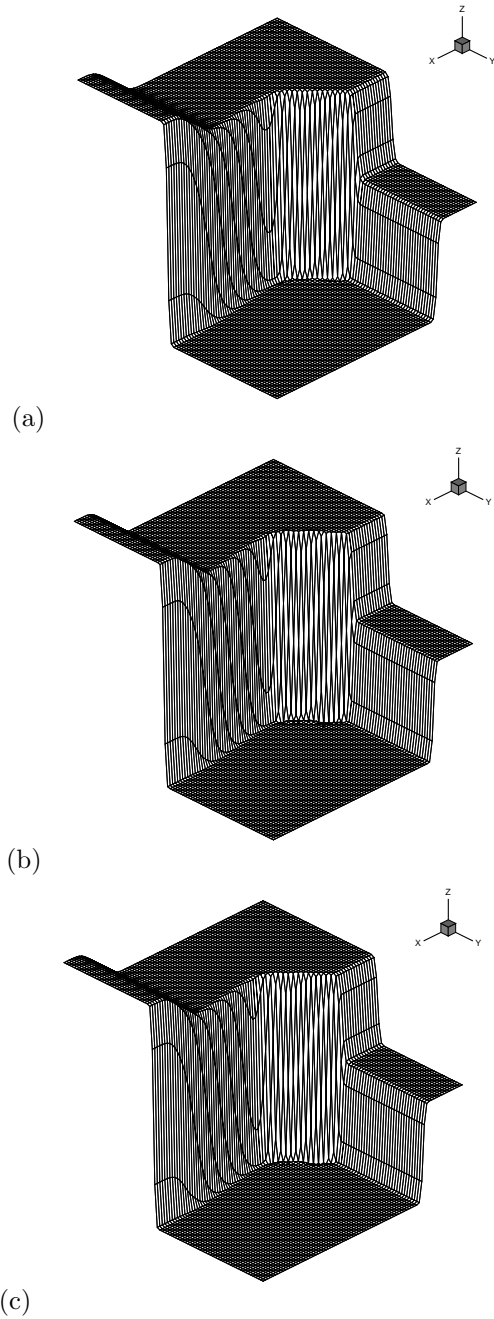
(a)

(b)

(c)

Fig. 4.1. *The central scheme results for the Burgers equation* (4.2) *evaluated with* 80×80 *cells and CFL* $= 0.475$ *at* $t = 1$. (a) *with* MM_1 *limiter;* (b) *with* MM_2 *limiter;* (c) *with UNO limiter.*
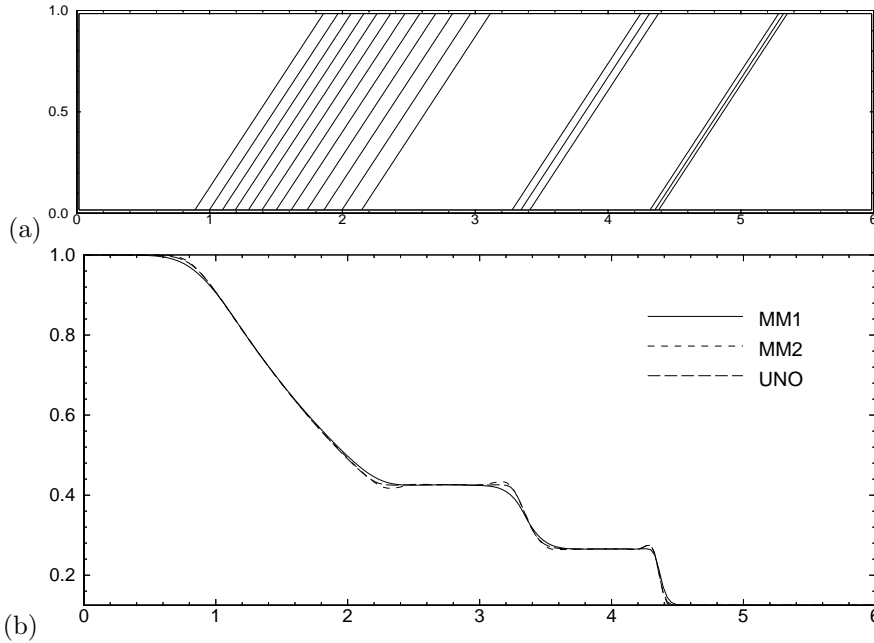
FIG. 4.2. *Oblique Sod's problem computed with the central scheme:* (a) *density contours computed with MM_2 limiter for initial data rotated with angle $\phi = \arctan 1$.* (b) *Density at $y = 0$ with rotated initial data, $\phi = \arctan 1$.*

- The two-dimensional computation is more sensitive to the type of limiter than in the one-dimensional framework [NT]. In the context of the double Mach reflection problem, the MM_2 seems to yield the sharper results.
- No effort was made to optimize the boundary treatment. The staggered stencils require a different treatment for even-odd cells intersecting with the boundaries. A more careful treatment is now studied in [TW]. The lack of boundary resolution could be observed at the bottom of the two Mach stems.

A key feature of our central scheme is its *efficiency*, due to the fact that all the central computations reported below are free of the time-consuming characteristic decompositions and dimensional splitting. This, in turn, is translated into the *fast, simple*, "two-lines" algorithm summarized in (2.15)–(2.16).

Table 4.2 quotes the CPU time, in seconds, for the computation of the two-dimensional Euler equations (4.3) subject to initial "sine" density wave:

$$(\rho_0, u_0, v_0, p_0) = (1 + 0.2\sin(\pi(x + y)), 1, -0.5, 1).$$

We record the timing for two versions of the central scheme. The Jacobian-free version employs a straightforward *componentwise* computation of the discrete derivatives $f(w)'$ and $g(w)^{\backprime}$, and we compare it with the other version which utilizes the Jacobians $A = f_w$ and $B = g_w$ to compute the discrete derivatives of the fluxes $f(w)' = Aw'$ and $g(w)^{\backprime} = Bw^{\backprime}$. We should emphasize that both versions yield comparable results, although, as expected, the latter version using the explicit Jacobians performs with slightly better resolution. Which of the two versions is preferable depends on several factors:

- Whether the exact Jacobians are available. For example, the gas-dynamics equation with *tabulated* pressure yields tabulated pointvalues of the flux (or
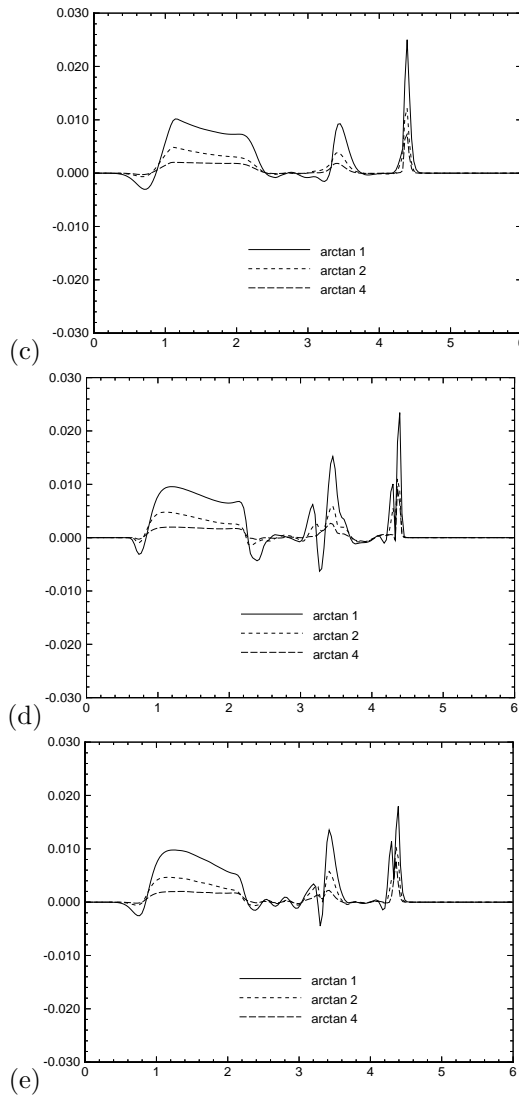
FIG. 4.3. *Figures* 4.2a, b *and* (c) *in this figure compare the two-dimensional oblique computation of the density,* ρ_ϕ, *vs. the rotated one-dimensional computation,* ρ_{1D}, *at* $y = 0$; $\rho_\phi - \rho_{1D}$ *computed with* (c) MM_1 *limiter,* (d) MM_2 *limiter,* (e) *UNO limiter.*

requires an implicit computation of such); its Jacobians could only be interpolated.

- The specific hardware configuration. In this context we note that the Jacobian-free version requires, instead, additional computation of limiters (of the fluxes evaluated at the midvalues). Associated with these limiters are switches whose speed is configuration-dependent.
- The *size* of the computed system. Thus, for example, the computations of the larger 7×7 MHD systems reported in [TW] perform much faster with the Jacobian-free version.

FIG. 4.4. *Double Mach reflection problem computed with the central scheme using* MM_1 *limiter with* 960×240 *cells and* CFL $= 0.475$ *at* $t = 0.2$. *(a) density, (b) x-velocity, (c) y-velocity, (d) pressure, (e) entropy.*

FIG. 4.5. *Double Mach reflection problem computed with the central scheme using* MM_2 *limiter with* CFL $= 0.475$ *at* $t = 0.2$: (a) *density computed with* 480×120 *cells*, (b) *density computed with* 960×240 *cells*, (c) *x-velocity computed with* 960×240 *cells*.

(d)

(e)

(f)
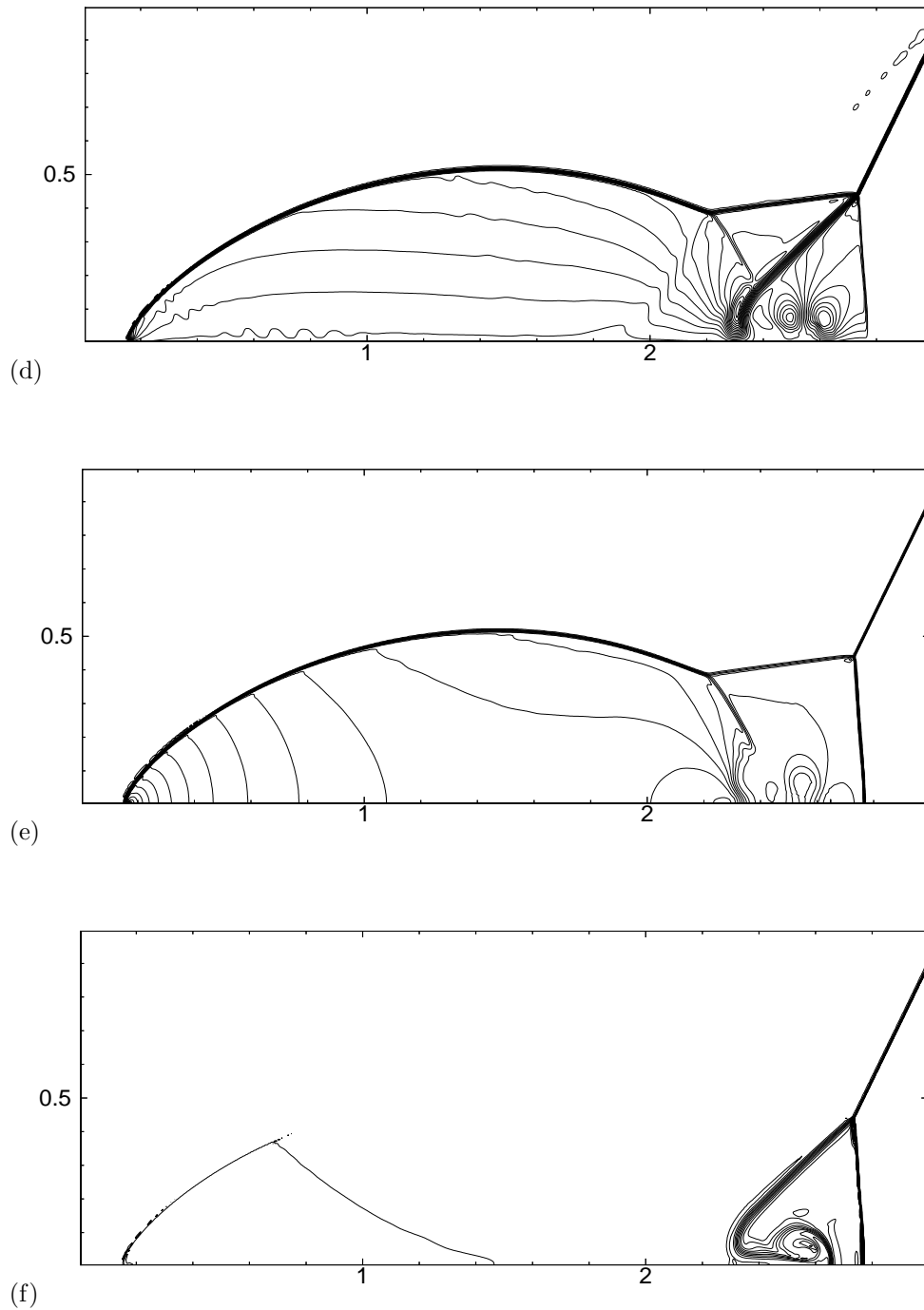
FIG. 4.5. *(Cont'd.) Double Mach reflection problem computed with the central scheme using* MM_2 *limiter with* 960×240 *cells and* CFL $= 0.475$ *at* $t = 0.2$: (d) *y-velocity,* (e) *pressure,* (f) *entropy.*
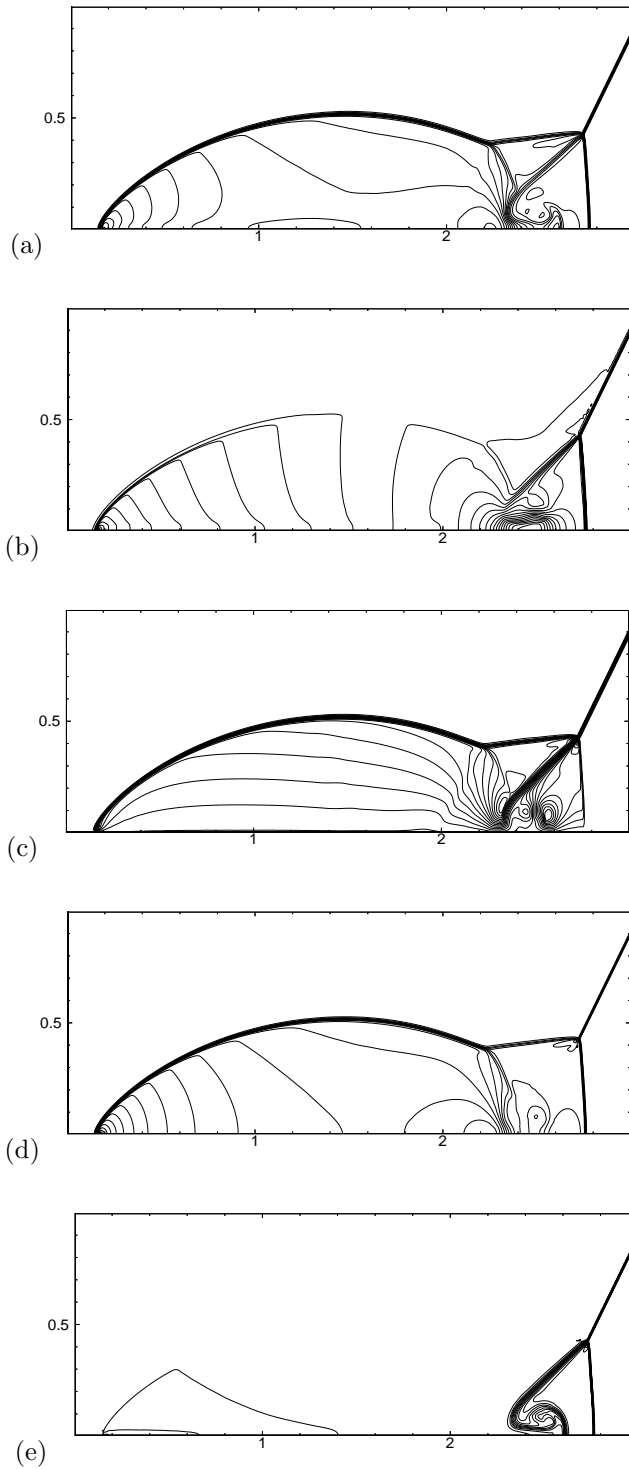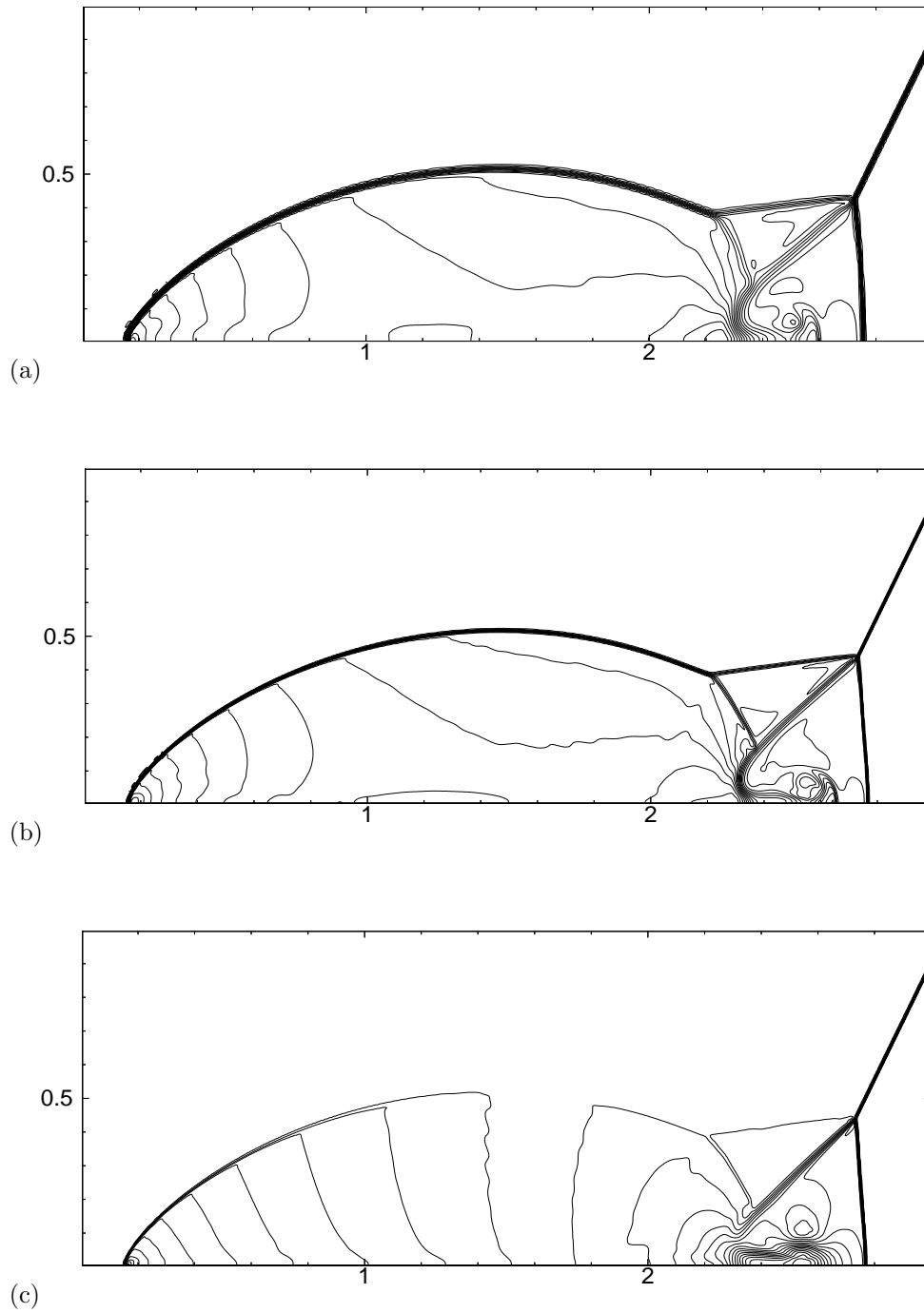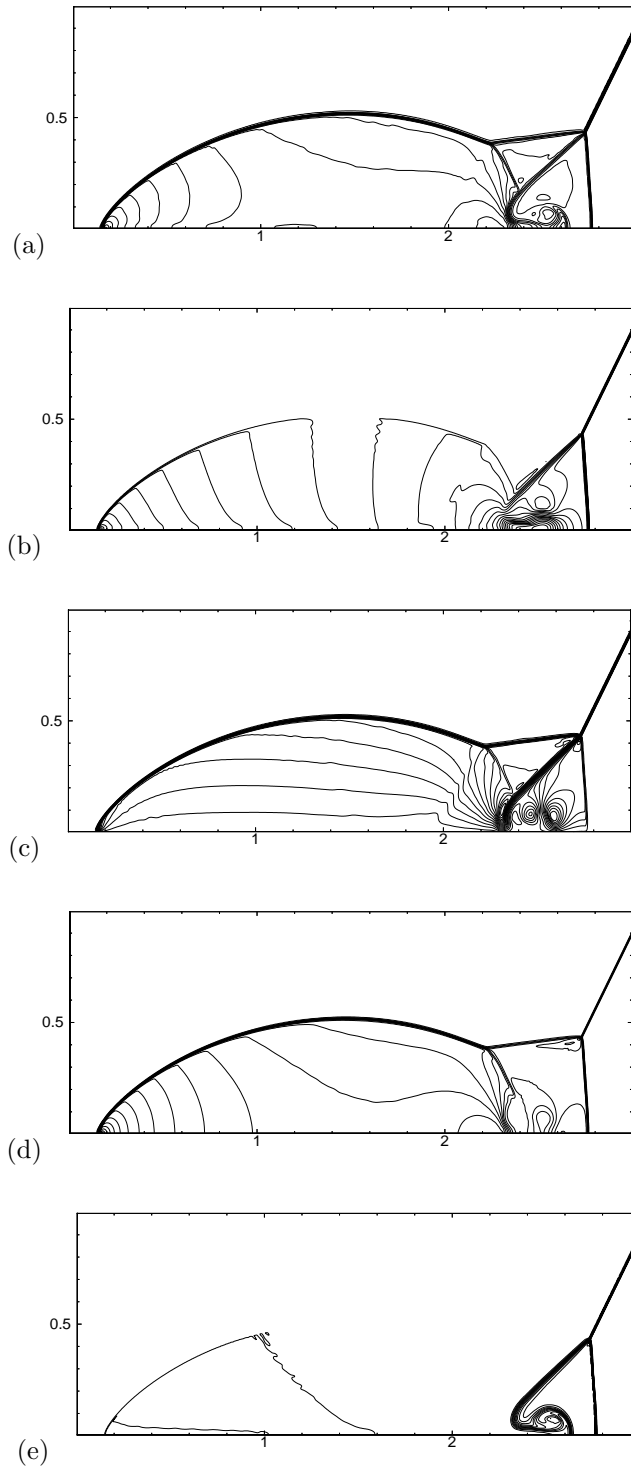
FIG. 4.6. *Double Mach reflection problem computed with the central scheme using UNO limiter with* CFL = 0.475 *at* t = 0.2: (a) *density*, (b) *x-velocity*, (c) *y-velocity*, (d) *pressure*, (e) *entropy*.

TABLE 4.2
CPU time in seconds for the central computation of the two-dimensional Euler system, with N_s cells in each spatial dimension and N_t temporal iterations, using various limiters.

N_s	N_t	MM_1 limiter	MM_2 limiter	UNO limiter	MM_1 limiter+ artificial compression
		CRAY C-90, with default compiler flags			
		$f(w)' = Aw'$, $g(w)^\backslash = Bw^\backslash$			
200	100	2.69	3.22	3.43	4.06
400	200	20.38	24.76	26.47	32.44
		$f(w)'$ and $g(w)^\backslash$ are obtained by componentwise limiters			
200	100	2.99	4.02	4.50	4.33
		SUN Sparc20 (60MHz, SuperSparc), compiled with "-r8 -fast -O3"			
		$f(w)' = Aw'$, $g(w)^\backslash = Bw^\backslash$			
100	50	10.79	14.29	16.28	18.30
200	100	92.27	119.13	136.98	159.26
		$f(w)'$ and $g(w)^\backslash$ are obtained by componentwise limiters			
200	100	133.93	188.88	223.49	203.34

4.3. Two-dimensional prologue: No dimensional splitting. Dimensional splitting (see, e.g., [RM]) is an effective, widely used tool for solving multidimensional problems by piecing them from one-dimensional problems—one dimension at a time. Still, in the context of nonlinear conservation laws, dimensional splitting encounters several limitations; we refer, for example, to the important results of Crandall and Majda in [CM].

In this subsection we provide one more piece of numerical evidence for the difficulties encountered with dimensional splitting, and with this we highlight the advantage of our "genuinely" multidimensional central scheme (2.15)–(2.16) in circumventing these difficulties. We consider the 2×2 system

$$(4.4) \qquad \begin{pmatrix} u_1 \\ u_2 \end{pmatrix}_t + \begin{pmatrix} \frac{u_1^2}{\sqrt{u_1^2+u_2^2}} \\ \frac{u_1 u_2}{\sqrt{u_1^2+u_2^2}} \end{pmatrix}_x + \begin{pmatrix} \frac{u_1 u_2}{\sqrt{u_1^2+u_2^2}} \\ \frac{u_2^2}{\sqrt{u_1^2+u_2^2}} \end{pmatrix}_y = 0.$$

The system (4.4) was introduced by Engquist and Runborg [ER] as part of a whole family of multiphase modeling for geometrical optics expansions. The first member of this family, (4.4), represents a one-phase solution consisting of a single ray of strength $g(r,t) := \sqrt{u_1^2 + u_2^2}$, located at a distance $r \equiv r(x,y)$ and an angle $\theta(x,y,t) := \arctan(u_2/u_1)$ relative to the (single) point source. We note that the system (4.4) is only *weakly* hyperbolic in the sense that its linearized symbol contains a 2×2 Jordan block; this seems to play an essential role in the difficulties associated with the computation of this system by dimensional splitting methods.

Following [ER], the system (4.4) is solved over the rectangle $0 \leq x \leq 1$, $0 \leq y \leq 2$, subject to zero initial conditions (to avoid overflow, we initialize $u_1 = u_{2|t=0} \equiv 10^{-12}$). The system is then activated by exact inflow boundary conditions along the left boundary, $x = 0$: in this case, these boundary values were taken from an exact point source solution, $g(r,t) = \max(0, (t-r)^3)/r$, located at $(-0.2, 1)$.

In Table 4.3 we quote the numerical results from [ER]: the (fully) two-dimensional Lax–Friedrichs scheme vs. the splitted versions based on the one-dimensional Lax–Friedrichs scheme [La], Godunov scheme [Go], and Nessyahu–Tadmor scheme (1.1)–(1.2), which were complemented with dimensional splitting. The best results were ob-

TABLE 4.3

Accuracy of Lax–Friedrichs, Godunov, and Nessyahu–Tadmor (1.1)–(1.2) *schemes (with and without dimensional splitting) for the one-phase geometric optics problem* (4.4) *at* $t = 0.85$.

Δx	Lax–Friedrichs				Godunov		Nessyahu–Tadmor	
	unsplitted		splitted		splitted		splitted	
L^1 results:	Error	Order	Error	Order	Error	Order	Error	Order
1/10	0.0778	-	0.01268	-	0.1130	-	0.048	-
1/20	0.0433	0.85	0.01543	-0.28	0.065	0.8	0.0357	0.43
1/40	0.0229	0.92	0.01226	0.33	0.0404	0.69	0.0181	0.98
1/80	0.0118	0.96	0.0079	0.63	0.0235	0.78	0.00839	1.11
1/160	0.00599	0.98	0.00454	0.8	0.013	0.85	0.0039	1.11
L^∞ results:	Error	Order	Error	Order	Error	Order	Error	Order
1/10	0.949	-	0.0662	-	3.038	-	0.278	-
1/20	0.397	1.26	0.07	-0.79	2.911	0.062	0.235	0.25
1/40	0.171	1.21	0.056	0.32	2.867	0.022	0.191	0.3
1/80	0.0771	1.15	0.0369	0.6	2.834	0.017	0.0857	1.15
1/160	0.0363	1.09	0.0215	0.78	2.815	0.01	0.0589	0.54

TABLE 4.4

Accuracy of the central approximation for the one-phase geometric optics problem (4.4) *with* MM_2 *limiter.*

Discrete derivatives	N	L^∞ error	L^∞ order	L^1 error	L^1 order
$f(w)' = Aw'$ $g(w)^{\backslash} = Bw^{\backslash}$	20	2.27e-2	-	6.19e-4	-
	40	8.12e-3	1.48	2.14e-4	1.53
	80	2.97e-3	1.45	7.38e-5	1.54
	160	1.10e-3	1.43	1.97e-5	1.91
Componentwise	20	2.83e-2	-	8.74e-4	-
	40	1.13e-2	1.32	2.89e-4	1.60
	80	4.51e-3	1.33	1.03e-4	1.49
	160	1.68e-3	1.42	2.86e-5	1.85

tained with the two-dimensional Lax–Friedrichs scheme, the forerunner for all central schemes: the unsplitted version achieves (close to) the expected first-order accuracy in both L^1- and L^∞-norms. The following three "splitted" versions which employ dimensional splitting yield less accurate results. Indeed, a considerable loss of accuracy is observed with the splitted version of the Lax–Friedrichs scheme.[2] The first-order upwind Godunov scheme, the forerunner for all upwind schemes, yields better L^1 errors; yet, measuring the L^∞ errors and consideration of the contour plots in [ER] shows that the splitted version of the Godunov scheme also *fails* to capture the full strength of the underlying computed rays. The same failure occurs with the splitted version of the second-order Nessyahu–Tadmor scheme: dimensional splitting causes the first-order L^1 errors and further loss of accuracy in terms of the L^∞ errors. In all three cases, this failure is attributed to the dimensional splitting.

These results should be contrasted with Table 4.4, where we quote the numerical results of the "genuinely" two-dimensional central scheme (2.15)–(2.16) using the MinMod limiter, MM_2. Both versions, with and without the exact Jacobians, achieve close to the expected second-order accuracy. Figure 4.7 confirms the high resolution of our central scheme.

_____

[2]We thank Olof Runborg for these results.
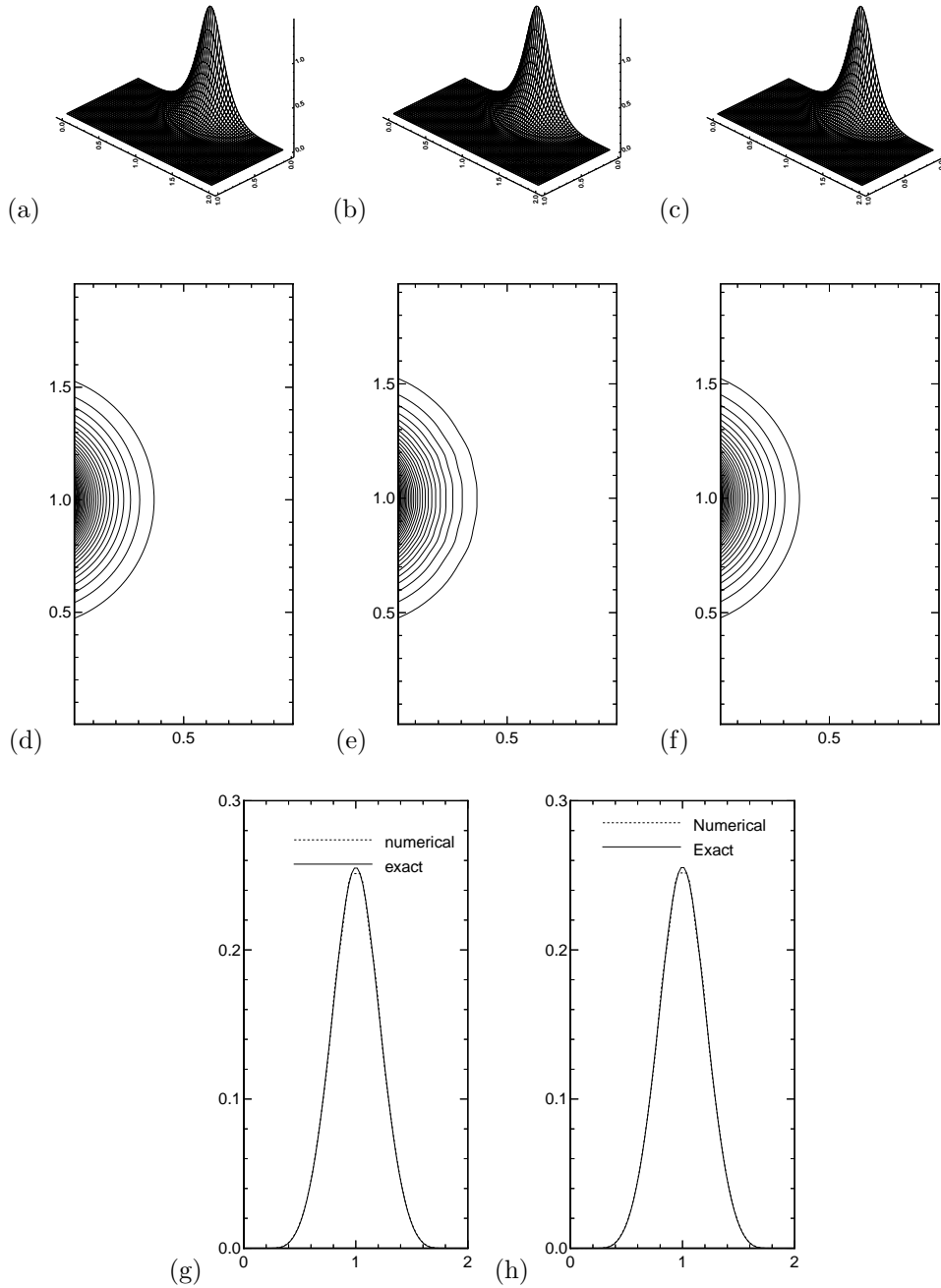
FIG. 4.7. *One-phase geometrical optics problem* (4.4), *computed by the two-dimensional central scheme with* 40×80 *cells and* CFL $= 0.475$ *at* $t = 0.85$. *Ray strength of exact solution in* (a) *is compared with central scheme computation with* MM_2 *limiter in* (b) *and with UNO limiter in* (c). *Exact contour plot in* (d) *is compared with* MM_2 *and UNO limiter computations in* (e) *and* (f), *respectively.* (g) *and* (h) *are vertical cuts at* $x = 0.2$ *computed with* MM_2 *and UNO limiters.*

5. Appendix.　A central code for two-dimensional Euler equations.

```
      subroutine EULER2D(nx,ny,dx,dy,cfl,gamma,theta,tf,u)
***********************************************************************
* INPUT  nx, ny:  # of cells in x-, y-direction
*        dx, dy:  step sizes in x-, y-direction
*        cfl: CFL #          gamma:  adiabatic constant of gas
*        tf:  final time
*        theta=1: MM1 limiter; =2: MM2 limiter; >2: UNO limiter.
*        u:  initial cell averages of conservative variables.
*            Supply entries of u((md+1):(nx+md),(md+1):(ny+md),4)
* OUTPUT u:  cell averages at final time "tf"
* REMARK  1. Reset "nxd","nyd" to adjust array dimensions.
*         2. Padded to each side of the computational domain are
*            "md" ghost cells, average values on which are
*            assigned by boundary conditions.
***********************************************************************
      parameter(md=3, nxd=400+2*md, nyd=400+2*md, mn=4)
      real u(nxd,nyd,mn), ux(nxd,nyd,mn), uy(nxd,nyd,mn)
      real f(nxd,nyd,mn), fx(nxd,nyd,mn)
      real g(nxd,nyd,mn), gy(nxd,nyd,mn)
      real v(nxd,nyd), du(nxd,2), df(nxd,2)

      xmin(a,b) = 0.5*(sign(1.,a)+sign(1.,b))*min(abs(a),abs(b))
      xmic(z,a,b) = xmin( z*xmin(a,b), 0.5*(a+b) )

      gm1 = gamma - 1.0
      tc = 0.0
      istop = 0

      do 1000 nt = 1, 10000
      do  999 io = 0, 1

* Periodic boundary condition in both x- & y-direction
      do 101 m = 1, mn
      do 100 i = 1, md
      do 100 j = md + 1, ny + md
        u(i,     j,m) = u(nx+i,j,m)
        u(nx + md+i,j,m) = u(md+i,j,m)
100   continue
      do 101 j = 1, md
      do 101 i = 1, nx + 2*md
        u(i,j,    m) = u(i,ny+j,m)
        u(i,ny + md+j,m) = u(i,md+j,m)
101   continue

* Compute f & g and maximum wave speeds "em_x, em_y".
* See (2.1) & (4.3).
      em_x = 1.e-15
      em_y = 1.e-15
      do 200 j = 1, ny + 2*md
      do 200 i = 1, nx + 2*md
        den = u(i,j,1)
        vex = u(i,j,2) / den
        vey = u(i,j,3) / den
        eng = u(i,j,4)
        pre = gm1 * ( eng - .5*den*( vex*vex + vey*vey ) )
        cvel = sqrt( gamma * pre / den )
        em_x = max( em_x, abs(vex) + cvel )
        em_y = max( em_y, abs(vey) + cvel )
        f(i,j,1) = den * vex
        f(i,j,2) = den * vex**2 + pre
        f(i,j,3) = den * vex * vey
        f(i,j,4) = vex * ( pre + eng )
        g(i,j,1) = den * vey
        g(i,j,2) = den * vex * vey
        g(i,j,3) = den * vey**2 + pre
        g(i,j,4) = vey * ( pre + eng )
200   continue

* Compute numerical derivatives "ux", "uy", "fx", "gy".
* See (3.1) & (4.1)
      do 330 m = 1, mn
      do 310 j = 3, ny + 2*md - 2
      do 301 i = 1, nx + 2*md - 1
        du(i,1) = u(i+1,j,m) - u(i,j,m)
301     df(i,1) = f(i+1,j,m) - f(i,j,m)
      do 302 i = 1, nx + 2*md - 2
        du(i,2) = du(i+1,1) - du(i,1)
302     df(i,2) = df(i+1,1) - df(i,1)
      if( theta .lt. 2.5 ) then
      do 303 i = 3, nx + 2*md - 2
        ux(i,j,m) = xmic( theta, du(i-1,1), du(i,1) )
303     fx(i,j,m) = xmic( theta, df(i-1,1), df(i,1) )
      else
      do 304 i = 3, nx + 2*md - 2
        ux(i,j,m)=xmin(du(i-1,1)+.5*xmin(du(i-2,2),du(i-1,2)),
```

```
     &              du(i,  1)-.5*xmin(du(i-1,2),du(i,  2)))
        fx(i,j,m)=xmin(df(i-1,1)+.5*xmin(df(i-2,2),df(i-1,2)),
     &              df(i,  1)-.5*xmin(df(i-1,2),df(i,  2)))
304   continue
      endif
310   continue
      do 320 i = 3, nx + 2*md - 2
      do 311 j = 1, ny + 2*md - 1
        du(j,1) = u(i,j+1,m) - u(i,j,m)
311     df(j,1) = g(i,j+1,m) - g(i,j,m)
      do 312 j = 1, ny + 2*md - 2
        du(j,2) = du(j+1,1) - du(j,1)
312     df(j,2) = df(j+1,1) - df(j,1)
      if( theta .lt. 2.5 ) then
      do 313 j = 3, ny + 2*md - 2
        uy(i,j,m) = xmic( theta, du(j-1,1), du(j,1) )
313     gy(i,j,m) = xmic( theta, df(j-1,1), df(j,1) )
      else
      do 314 j = 3, ny + 2*md - 2
      uy(i,j,m)=xmin(du(j-1,1)+.5*xmin(du(j-2,2),du(j-1,2)),
     &            du(j,  1)-.5*xmin(du(j-1,2),du(j,  2)))
      gy(i,j,m)=xmin(df(j-1,1)+.5*xmin(df(j-2,2),df(j-1,2)),
     &            df(j,  1)-.5*xmin(df(j-1,2),df(j,  2)))
314   continue
      endif
320   continue
330   continue

* Compute time step size according to the input CFL #.
      if(io.eq.0) then
        dt = cfl / max( em_x/dx, em_y/dy )
        if( ( tc + 2.*dt ) .ge. tf ) then
          dt = 0.5 * ( tf - tc )
          istop = 1
        endif
      endif
      dtcdx2 = 0.5 * dt / dx
      dtcdy2 = 0.5 * dt / dy

* Compute the flux values of f & g at half time step.
* See (2.15) & (2.16).
      do 400 j = 3, ny + 2*md - 2
      do 400 i = 3, nx + 2*md - 2
        den = u(i,j,1) - dtcdx2*fx(i,j,1) - dtcdy2*gy(i,j,1)
        xmt = u(i,j,2) - dtcdx2*fx(i,j,2) - dtcdy2*gy(i,j,2)
        ymt = u(i,j,3) - dtcdx2*fx(i,j,3) - dtcdy2*gy(i,j,3)
        eng = u(i,j,4) - dtcdx2*fx(i,j,4) - dtcdy2*gy(i,j,4)
        pre = gm1 * ( eng - .5 * ( xmt*xmt + ymt*ymt ) / den )
        f(i,j,1) = xmt
        f(i,j,2) = xmt * xmt / den + pre
        f(i,j,3) = xmt * ymt / den
        f(i,j,4) = xmt / den * ( pre + eng )
        g(i,j,1) = ymt
        g(i,j,2) = xmt * ymt / den
        g(i,j,3) = ymt * ymt / den + pre
        g(i,j,4) = ymt / den * ( pre + eng )
400   continue

* Compute the values of "u" at the next time level. See (2.16).
      do 510 m = 1, mn
      do 501 j = md + 1 - io, ny + md - io
      do 501 i = md + 1 - io, nx + md - io
        v(i,j) =   0.25 * ( u(i,j,  m) + u(i+1,j,  m)
     &                   + u(i,j+1,m) + u(i+1,j+1,m) )
     &         + 0.0625 * ( ux(i,j,  m) - ux(i+1,j,  m)
     &                   + ux(i,j+1,m) - ux(i+1,j+1,m)
     &                   + uy(i,j,  m) + uy(i+1,j,  m)
     &                   - uy(i,j+1,m) - uy(i+1,j+1,m) )
     &         + dtcdx2 * (  f(i,j,  m) -  f(i+1,j,  m)
     &                   +  f(i,j+1,m) -  f(i+1,j+1,m) )
     &         + dtcdy2 * (  g(i,j,  m) +  g(i+1,j,  m)
     &                   -  g(i,j+1,m) -  g(i+1,j+1,m) )
501   continue
      do 502 j = md + 1, ny + md
      do 502 i = md + 1, nx + md
502     u(i,j,m) = v(i-io,j-io)
510   continue

      tc = tc + dt
999   continue
      if(istop.eq.1 ) goto 1001
1000  continue

1001  return
      end
```

REFERENCES

[AV]   P. ARMINJON AND M. C. VIALLON, *Généralisation du schéma de Nessyahu-Tadmor pour une équation. hyperbolique à deux dimensions d'espace*, C.R. Acad. Sci. Paris, 320 (1995), pp. 85–88.

[BS]   F. BEREUX AND L. SAINSAULIEU, *A Roe-type Riemann solver for hyperbolic systems with relaxation based on time-dependent wave decomposition*, Numer. Math., 77 (1997), pp. 143–185.

[CM]   M. CRANDALL AND A. MAJDA, *The method of fractional steps for conservation laws*, Numer. Math., 34 (1980), pp. 285–314.

[Er]   G. ERBES, *A high-resolution Lax-Friedrichs scheme for Hyperbolic conservation laws with source term. Application to the Shallow Water equations*, J. Comput. Phys., to appear.

[EO]   B. ENGQUIST AND S. OSHER, private communication, 1996.

[ER]   B. ENGQUIST AND O. RUNBORG, *Multi-phase computations in geometrical optics*, J. Comput. Appl. Math., 74 (1996), pp. 175–192.

[Go]   S. K. GODUNOV, *A finite difference method for the numerical computation of discontinuous solutions of the equations of fluid dynamics*, Mat. Sb., 47 (1959), pp. 271–290.

[Ha1] A. HARTEN, *The artificial compression method for the computation of shocks and contact discontinuities:* I. *Single conservation laws*, Comm. Pure Appl. Math., 39 (1977), pp. 611–638.

[Ha2] A. HARTEN, *High resolution schemes for hyperbolic conservation laws*, J. Comput. Phys., 49 (1983), pp. 357–393.

[HO]   A. HARTEN AND S. OSHER, *Uniformly high order accurate non-oscillatory scheme.* I, SIAM J. Numer. Anal., 24 (1982), pp. 229–309.

[Hu]   H. T. HUYNH, *A piecewise-parabolic dual-mesh method for the Euler equations*, AIAA-95-1739-CP, The 12th AIAA CFD Conf., 1995.

[JS]   G.-S. JIANG AND C.-W. SHU, *Efficient implementation of weighted ENO schemes*, J. Comput. Phys., 126 (1996), pp. 202–228.

[La]   P. D. LAX, *Weak solutions of non-nonlinear hyperbolic equations and their numerical computations*, Comm. Pure Appl. Math., 7 (1954), pp. 159–193.

[LL]   X.-D. LIU AND P. D. LAX, *Positive schemes for solving multi-dimensional hyperbolic systems of conservation laws*, CFD Journal, 5 (1996), pp. 1–24

[LO]   X.-D. LIU AND S. OSHER, *Non-oscillatory high order accurate self similar maximum principle satisfying shock capturing schemes.* I, SIAM J. Numer. Anal., 33 (1996), pp. 760–779.

[LT]   X.-D. LIU AND E. TADMOR, *Third order non-oscillatory central scheme for Hyperbolic conservation laws*, UCLA CAM Report 96-42; Numer. Math., to appear.

[MO]   A. MAJDA AND S. OSHER, *Propagation of error into regions of smoothness for accurate difference approximations to hyperbolic equations*, Comm. Pure Appl. Math., 30 (1977), pp. 671–705.

[NT]   H. NESSYAHU AND E. TADMOR, *Non-oscillatory central differencing for hyperbolic conservation laws*, J. Comput. Phys., 87 (1990), pp. 408–448.

[OT]   S. OSHER AND E. TADMOR, *On the convergence of difference approximating to scalar conservation laws*, Math. Comp., 50 (1988), pp. 15–51.

[RM]   R. D. RICHTMYER AND K. W. MORTON, *Difference Methods for Initial Value Problems*, 2nd ed., Interscience, New York, 1967.

[Sa2] R. SANDERS, private communication, 1995.

[SW]   R. SANDERS AND A. WEISER, *A high resolution staggered mesh approach for nonlinear hyperbolic systems of conservation laws*, J. Comput. Phys., 1010 (1992), pp. 314–329.

[Sw]   P. SWEBY, *High resolution schemes using flux limiters for hyperbolic conservation laws*, SIAM J. Numer. Anal., 5 (1984), pp. 995–1011.

[So]   G. SOD, *A survey of several finite difference methods for systems of nonlinear hyperbolic conservation laws*, J. Comput. Phys., 22 (1978), pp. 1–31.

[TW]   E. TADMOR AND C. C. WU, *Central scheme for the multidimensional MHD equations*, in preparation.

[WC]   P. WOODWARD AND P. COLELLA, *The numerical simulation of two-dimensional fluid flow with strong shocks*, J. Comput. Phys., 54 (1988), pp. 115–173.